INVESTIGATION ON LOCAL SCOUR BEHIND COASTAL STRUCTURES DUE TO TSUNAMI OVERFLOW

津波越流による海岸構造物背後の局所洗掘に関する検討

A dissertation

by

Mustarakh GELFI

Supervisor: Prof. Takayuki SUZUKI

Civil Engineering Department

Graduate School of Urban Innovation

Yokohama National University

September 2023

Abstract

In this study, the existing predictive landward structure scour depth equation proposed by Jayaratne et al. (2016) was examined in the context of sediment size effects (d_{50}) and structural porosity (n). The equation, which considers parameters such as dike height (H_d), inundation depth (h), and landward structural slope (θ), has shown potential in predicting scour depth induced by overflowing tsunami waves.

However, careful attention is required when implementing the predictive depth equation due to the simplification of the fitted coefficient (λ). To investigate the sediment size effect, laboratory experiments were conducted using three different sediment sizes, with each test repeated three times for a total of nine test runs. To investigate the effect of structural porosity (n), 5 stone sizes (constitute 5 different porosities) were dumped to the structural model. The focus was on analyzing the scour depth (D_s) to gain a detailed understanding of landward toe scour behavior in relation to d_{50} and n.

The findings of the study revealed an inverse proportional relationship between D_s and the grain size within the range of non-cohesive sand samples (d_{50}= 0.30-2.56 mm). It is also found that porous structure tends to shift the scour profile to the structural direction. Higher porosity of the structure reduces the scour depth linearly. Based on these findings, the study proposes revising the fitted coefficient ($\lambda_{n,s}$) to incorporate the sediment size and structural porosity effects in the application of the existing scour depth predictive equation of Jayaratne et al. (2016).

The study also compared the simulation results of XBeach against experimental data (related to sediment size only) to evaluate its performance. The model showed good agreement between the model and experimental data in terms of water level variation, although the simulated flow velocity slightly overestimated the observed values. It is worth noting that in very short-time scale phenomena like landward scour, the model's sensitivity to the governing equation of sediment transport becomes more apparent.

The model also successfully reproduced the morphodynamical shape of the scour hole, indicating its capability to capture the overall behavior of the landward scour process. However, the scour depth (D_s), as observed in other studies for extreme overflowing conditions, was found to be overestimated by the model. To improve the results, the study implemented an artificial erosion limiter by activating soil dilatancy effects. This enhancement, aimed at reducing the overestimation of scour depth, particularly improved the accuracy of erosion volume (V_{err}) predictions. Employing a higher bed shear stress, represented by the Manning coefficient, holds promising potential for enhancing outcomes, particularly in terms of decreasing flow velocity within the scour medium and reducing scour depth. In physical terms, the elevation of stress can be interpreted as a heightened dissipation of energy during laboratory experiments involving water and the interaction with model structures. This encompasses the loss of water towards the periphery of the structure and within the system of erodible materials.

In conclusion, this study emphasizes the importance of considering sediment size (d_{50}) and structural porosity (n) effects in predicting landward structure scour depth and highlights the need to revise the fitted coefficient to improve the accuracy of the existing predictive equation. It also demonstrates the capability of XBeach to simulate the morphodynamics of landward scour, although improvements are needed to accurately predict scour depth. The study highlights the importance of considering factors such as artificial erosion limiters and sediment transport equations in modeling landward scour phenomena.

Acknowledgements

I would like to express my deepest gratitude to the many individuals who have supported and encouraged me throughout this journey. Their unwavering belief in my abilities has been invaluable, and I am truly grateful for their presence in my life. I would like to acknowledge and extend my heartfelt thanks to my family, professors, and friends.

I would also like to express my gratitude to all the individuals who have directly or indirectly contributed to my academic pursuits. To the faculty members and administrative staff at Yokohama National University, thank you for your support and for creating an environment conducive to learning.

I hope you enjoy reading my magnum opus during my academic journey.

Table of contents

List of figures

List of tables

Chapter 1
Introduction

1. Introduction

1.1 Background

Scour issues have persisted within civil engineering infrastructure for an extended duration. Concerns arise regarding the stability of foundations and decks due to scouring around bridge piers in rivers. Similarly, in coastal areas, scouring at the seaward base of breakwaters and seawalls has the potential to trigger structural failure. Presently, the swift advancement of offshore wind energy infrastructure has also impacted the examination of scouring around reinforced concrete piles.

Landward coastal structure scour refers to a specific type of local scour that occurs at the backside of coastal structures. In the context of the 2011 Great East-Japan (Tohoku) earthquake and tsunami, it was discovered that landward scour played a significant role in the failure of coastal defenses. The tsunami's exceptionally high-water depth resulted in the overflow of coastal defenses, leading to the generation of landward scours. This scour hole, situated landward, was the primary cause of the complete failure of 50% of the sea defenses in the Tohoku region.

Sea and coastal defenses are typically constructed to withstand wave forces coming from the sea. Consequently, scour protection measures are designed to be located at the seaward toe of these structures. However, during a tsunami, the incoming waves can overwhelm the defenses, resulting in the establishment of scour on the landward side. Unfortunately, the landward side of coastal structures is often left without proper protection measures in place.

Nicholas et al, Chen et al, and Jayaratne et al have put forth predictive scour equations specifically for the land side of coastal structures, also known as landward scour. The former researchers proposed an empirical relation to estimate the depth of scour for rectangular structures. On the other hand, the latter researchers examined sloping structure models and conducted post-investigations of scour in various cities within the Tohoku area, considering the 2011 tsunami event.

The predictive equation for landward scour developed by Jayaratne et al. considers the ratio of relative overflowing water pressure (D_s) to relative scour depth (H_d), and is expressed as follows:

$$\frac{D_s}{H_d} = \lambda \times \exp\left(-\frac{\sqrt{H_d}}{2.5\,\lambda\,\sqrt{h}\sin\theta}\right) \quad (1\text{-}1)$$

where, D_s is the scour depth (m), H_d is the coastal structure height (m), h is the inundation depth (m), θ is the slope of structure, λ is the fitted coefficient (=0.85).

The fitted coefficient (λ) in Equation 1 serves as a simplification of all the uncertainties inherent in the equation. While it helps to keep the predictive equation straightforward, it can pose issues when specific field conditions are taken into account, such as sediment size and structural porosity. In the experiments conducted by Jayaratne et al (2016), a single-size sediment dimension and impermeable model structures were used, resulting in a λ value of 0.85.

Reported measurements of scour depths around coastal defensive structures in several cities in the Tohoku area are as follows:

1. In Ishinomaki, Iwanuma, and Yamamoto cities (Miyagi prefecture), the observed scour depths ranged from 1.14 m to 2.5 m.
2. In Soma city (Fukushima prefecture), the measured scour depth was approximately 3.6 m.
3. In Watari city (Miyagi prefecture), the observed scour depths ranged from 2.37 m to 4.06 m.

However, it was also observed that the sediment characteristics, specifically the median grain size (d_{50}), varied across the different cities. In Ishinomaki, Iwanuma, Yamamoto, and Watari, the d_{50} values were 0.65 mm, 0.67 mm, 0.74 mm, and 0.86 mm, respectively. These sizes indicate medium-sized particles. On the other hand, in Soma, the d_{50} value was 0.22 mm, which indicates the presence of fine particles.

Moreover, most of the experiments conducted related to this topic before considered only impermeable (porosity (n)= 0) which used wood, steel, or acrylic as materials for coastal structures model. In the field, the structure is of course having some permeability which presumably will influence the developed scour profiles.

XBeach is indeed a widely used and respected model for simulating coastal processes and morphology. Its capabilities extend to analyzing wave-driven shoreline evolution, including interactions with beach and dune systems. One of the main advantages of XBeach is its ability to simulate the highly nonlinear and complex processes involved in shoreline dynamics, such as wave breaking, swash zone hydrodynamics, and sediment transport.

One of the reasons for the popularity of XBeach is its user-friendly interface, which allows for easy setup and adjustment of model parameters and conditions. This flexibility makes it suitable for a wide range of applications and research studies. Additionally, XBeach has been extensively validated against both laboratory and field data, demonstrating its ability to accurately represent real-world coastal systems.

However, when it comes to simulating local scour behind structures specifically induced by tsunamis, the validation becomes more challenging. Researchers have made attempts to validate the model's hydrodynamic and morphodynamic performance, particularly in the context of storms, and have reported qualitatively good agreement. However, it has been observed that XBeach tends to overestimate erosion volumes in scenarios with high overtopping rates and large flow velocities during extreme events like storms, hurricanes, and tsunamis.

The objectives of the paper discussed are to test XBeach's ability to accurately simulate landward scour phenomena and compare its predictions with available experimental data from Gelfi et al (2022). Additionally, the study aims to identify the key sensitivity factors that influence the model's results and proposes potential improvements to the default setup of XBeach to enhance its accuracy in predicting landward scour.

Therefore, the objective of this research is to examine the impact of sediment size (d_{50}) and structural porosity (n) on the predictive equation for landward toe scour depth. The study specifically focuses on the influence of the overflowing mass of water over the structure, as it is recognized as the primary mechanism in the context of landward toe scour during tsunami waves. Furthermore, the study also tried to investigate XBeach's ability to accurately simulate landward scour phenomena and compare its predictions with available experimental data.

1.2 Objectives

Oversimplification of the existing predictive equation of the local scour behind coastal structures presumably has an impact on the accuracy of the prediction. Moreover, existing experiments are mostly considering impermeable condition of the model structures while the structure has porosity. Therefore, the aims of this study are:

1. To elaborate fitted coefficient ($\boldsymbol{\lambda}$) on the predictive equation in relation to sediment size (d_{50}).
2. To explore the applicability analysis of the phenomenon in XBeach model.
3. To further elaborate the existing predictive equation and then see the effect of permeable structure (n).

1.3 Research frameworks

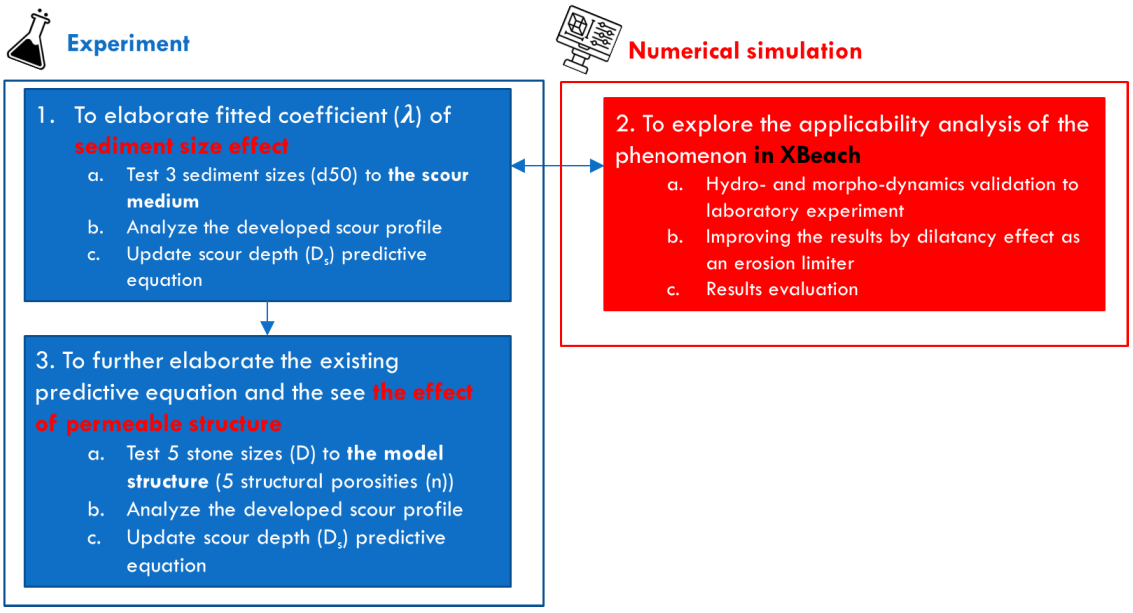

Figure 1.1 Research frameworks

Figure 1.1 displays the research framework of this study. This study is conducted to achieve certain objectives which are related to investigating the effect of sediment variability on the developed local scour behind the structures. By means of experimental works, we hope to gain valuable data especially related to scour depth and use it to improve existing predictive equations (Chapter 4).

XBeach is used to confirm the available dataset (experiment) by way of numerical modeling and investigate valuable insight on how to apply the phenomenon numerically (Chapter 5). Further investigation through experiment is conducted to elaborate the effect of structural porosity on the developed landward scour. The result will be used to further improve the existing predictive equation (Chapter 6).

1.4 Research limitations

Some simplifications related to methodology and results interpretation of the research were realized leading to results bias. In the following, some limitations of the study are:

1. The laboratory works mainly focus on the impact on the overflowing flow of tsunami wave in the limited time span.
2. The laboratory was conducted in 2D flume, therefore mainly related cross-shore flow and sediment transport. The longshore flow effect was neglected.

3. The study was done relatively in small scale as compared to real life dimension. Although scaling rule was obeyed, there is still potential bias due to sediment dimension.
4. As for numerical model XBeach, the model is based on averaged depth water flow. Therefore, there is potential discrepancy of the result comparison especially in velocity interpretation.

Chapter 2

Literature Review

2. Literature Review

2.1 Local scour behind the structures

MLIT (Ministry of Land, Infrastructure, Transport, and Tourism) and Mitobe et al (2014). have extensively documented significant erosion occurring on the leeside of coastal defense structures because of the 2011 Tohoku Earthquake and Tsunami. Landward scour, as described by Jayaratne et al (2016), was identified as a major contributing factor to the destruction of structures in the Tohoku region. To investigate this phenomenon, laboratory experiments were conducted, and an empirical equation was proposed to predict landward scour depth based on various factors related to wave hydrodynamics. Gelfi et al (2022) further extended this equation by incorporating sediment properties, again based on laboratory experimentation.

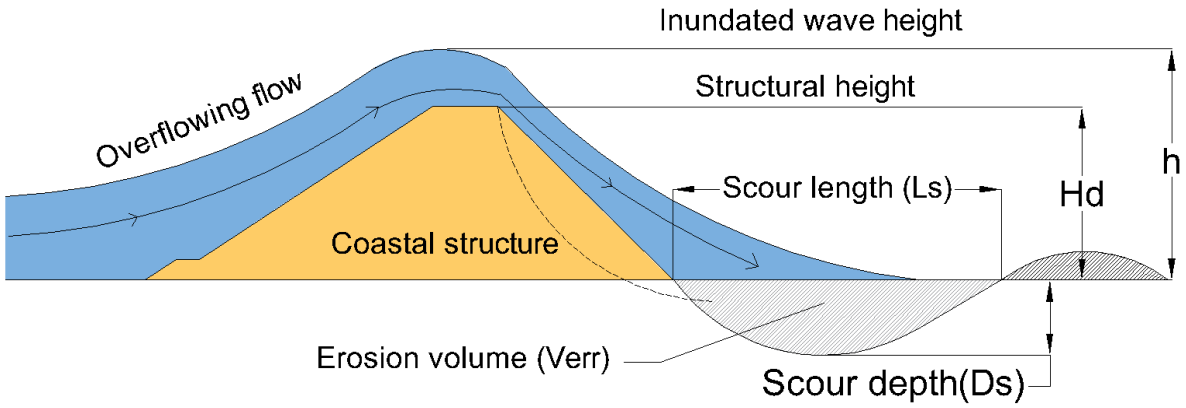

Figure 2.1 Schematic view of local scour behind the structures

Figure 2.1 illustrates a typical overflowing process observed during a tsunami, which leads to the formation of an erosion hole on the leeside of a structure, known as landward scour. Several parameters are associated with this phenomenon, including structure height (H_d), inundated wave height (h), scour depth (D_s), and scour length (L_s). These parameters play crucial roles in understanding and predicting the extent and characteristics of landward scour, which is essential for effective coastal defense planning and design.

Table 2.1 Field data of 2011 Tohoku Tsunami

Location	h (m)	V_p (m/s)	θ	H_d (m)	D_s (m)
Ishinomaki port	6	9.2	70.3	1.4	1.22 1.66 1.29 1.16 1.14
Soma	6.8	9.8	35	4.37	2.83 3.87 3.60 3.50
Watari	7.6	10.36	77.7	4.6	4.06 2.37 2.75
Iwanuma	5.7	8.97	54.6	5.76	2.50 1.09 2.00 1.90
Yamamoto	7.4	10.22	34.8	5.29	1.86 1.40 1.65

Table 2.1 shows field data of tsunami's hydrodynamics (inundation depth (h) and prototype velocity (V_p)), structural dimension (dike height (H_d) and structural slope (θ)) and scour depth (D_s) of 2011 event in Tohoku area (Japan). The cities of field data include Ishinomaki, Soma, Watari, Iwanuma, and Yamamoto cities. The data is a combination of field measurement (scour depth and dike dimension data) and secondary data interpretation (recorded video interpolation). The inundation depths and tsunami velocities data were from recorded data.

2.2 XBeach model

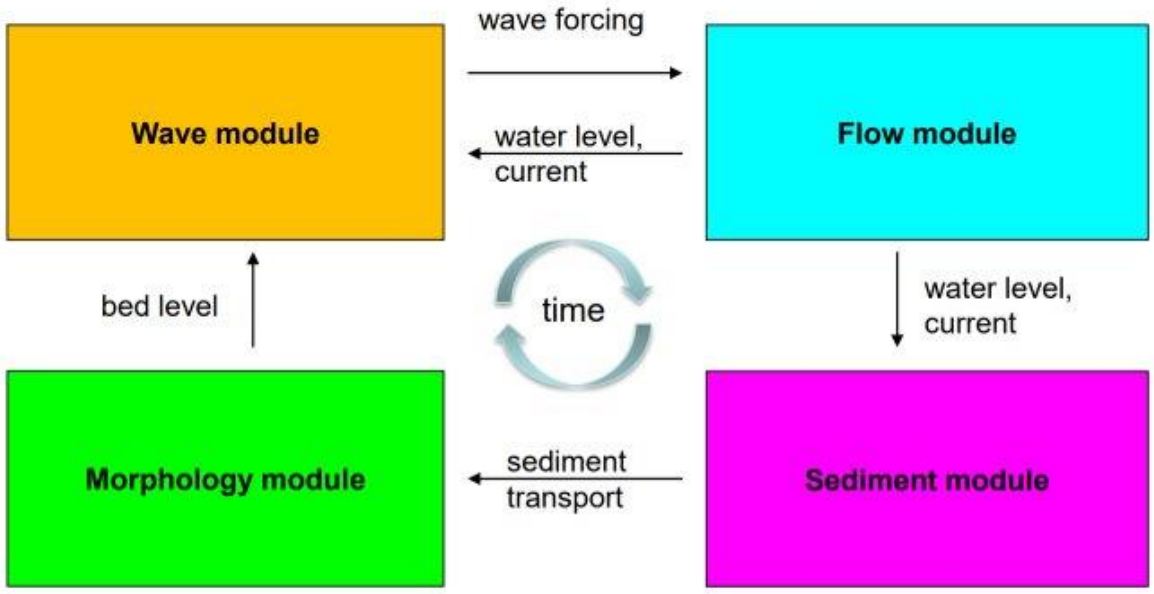

Figure 2.2 XBeach modeling scheme

XBeach is a renowned and extensively utilized model for simulating coastal processes and morphology. It offers a comprehensive set of tools for analyzing the evolution of shorelines driven by waves and their interactions with beaches and dunes. The popularity of XBeach stems from its capacity to simulate highly nonlinear and intricate processes involved in shoreline evolution, including wave breaking, hydrodynamics in the swash zone, and sediment transport.

The model boasts a user-friendly interface and provides flexibility in setting up and adjusting model parameters and conditions. It has undergone rigorous validation against diverse laboratory and field data, showcasing its ability to accurately replicate the behavior of real-world coastal systems. The combination of accuracy, flexibility, and user-friendliness has solidified XBeach as one of the most widely employed models in the field of coastal modeling. **Figure 2.2** shows XBeach modeling scheme in which it calculates wave, flow, sediment, and morphology modules in the change of time.

2.3 Wave action equation

XBeach employs a coupled stochastic (phase-averaged) spectral wave model to simulate storm-induced waves and a non-linear shallow water model for infra-gravity waves. The model solves short-wave processes based on the wave action equation, considering the stochastic behavior of waves. To enhance the accuracy of wave modeling, XBeach incorporates empirical formulations that have been calibrated using field data and laboratory

measurements. The short-wave action balance is governed by a mathematical equation that captures the interactions between waves, currents, and sediment transport as follows,

$$\frac{\partial A}{\partial t}+\frac{\partial c_x A}{\partial x}+\frac{\partial c_y A}{\partial y}+\frac{\partial c_\theta A}{\partial \theta}=-\frac{D_w+D_f+D_v}{\sigma} \quad (2\text{-}1)$$

where c is wave action propagation speed. Wave dissipation processes consist of breaking (D_w), bottom friction (D_f), and vegetation (D_v). θ and σ represent the angle of incident and the intrinsic frequency respectively. In which the wave action A is formulated as:

$$A(x,y,t,\theta)=\frac{S_w\ (x,\ y,t,\theta)}{\sigma\ (x,\ y,t,\theta)} \quad (2\text{-}2)$$

where S_w represents the wave energy density.

2.4 Sediment transport formulas

In XBeach, we can opt to use 3 available sediment transport formulations through caller function 'form', which are (i) soulsby-vanrijn, (ii) vanthiel-vanrijn, and (iii) vanrijn1993. In the first equation, the wave and current are averagely calculated. Furthermore, drag coefficient (C_d) is also calculated. The equilibrium sediment concentrations (Ceq) formulated according to:

$$C_{eq,b}=\frac{A_{sb}}{h}\left(\sqrt{v_{mg}^2+\frac{0.018u_{rms,2}^2}{C_d}}-U_{cr}\right)^{2.4} \quad (2\text{-}3)$$

$$C_{eq,s}=\frac{A_{ss}}{h}\left(\sqrt{v_{mg}^2+\frac{0.018u_{rms,2}^2}{C_d}}-U_{cr}\right)^{2.4} \quad (2\text{-}4)$$

where h, v_{mg}, and u_{rms} represent wave height, Eulerian velocity magnitude, and orbital velocity respectively. Subscripts b and s refer to mode of transport of bed and suspended loads respectively. A_{sb}, A_{ss}, and U_{cr} are bed load coefficient, suspended load coefficient, and critical velocity respectively.

The second equation is the default equation used by Xbeach. In this equation, wave and current are calculated separately. The drag coefficient (C_d) is not determined. The equilibrium sediment concentrations (C_{eq}) formulated as follow:

$$C_{eq,b}=\frac{A_{sb}}{h}\left(\sqrt{v_{mg}^2+0.64u_{rms}^2}-U_{cr}\right)^{1.5} \quad (2\text{-}5)$$

$$C_{eq,s} = \frac{A_{ss}}{h}\left(\sqrt{v_{mg}^2 + 0.64u_{rms}^2} - U_{cr}\right)^{2.4} \quad (2\text{-}6)$$

In the last equation, a reference height is setup to distinguish the bed load and suspended load transport formulas. The bed load (S_b) and suspended load reference concentration (c_a) are formulated as follow:

$$S_b = 0.006\rho_s w_s D_{50} M^{0.5} {M_e}^{0.7} \quad (2\text{-}7)$$

$$c_a = 0.015\rho_s \frac{D_{50}{T_a}^{1.5}}{\alpha {D_*}^{0.3}} \quad (2\text{-}8)$$

In which the sediment mobility number due to waves and currents (M):

$$M = \frac{{v_e}^2}{(s-1)gd_{50}} \quad (2\text{-}9)$$

Where ve and s are effective velocity and specific gravity (ρ_s/ρ) respectively.

Chapter 3

Methodology

3. Methodology

3.1 Laboratory works

3.1.1 Experimental setup

The analysis primarily focused on conducting clear water scour experiments. This was because during tsunami overflow, the sediment supply from the seaward side of the model structure is typically removed. As a result, the moveable bed condition was created solely on the landward side of the structure, while the other parts were constructed as impermeable.

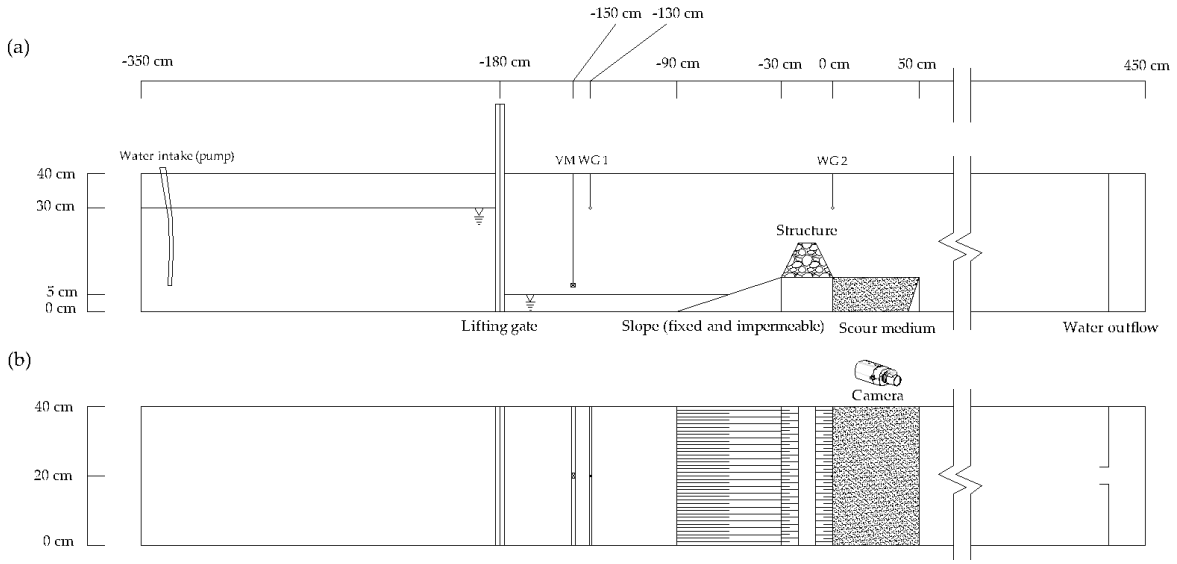

Figure 3.1 Laboratory experiment setup: a) side view; b) plan view

The experiments were carried out within a 2D wave flume with overall dimensions of 16.5 meters in length, 0.4 meters in width, and 0.4 meters in depth (**Figure 3.1**). However, for the dam-break gate, model structure, and sediment box, only a length of 4.4 meters within the flume was utilized. The starting point of the horizontal coordinate (x = 0 cm) was positioned at the landward tip of the structure, with positive values extending landward. The vertical direction was assigned with the reference point at the flume bed (z = 0 cm).

To simulate a tsunami-like wave, a dam-break mechanism was employed. Initially, a significant amount of water mass was accumulated behind a gate. Subsequently, the gate was released, allowing the water to flow towards the structure-scour area. The dam-break wave generation mechanism demonstrated a satisfactory agreement with the field data from the 2004 Sumatra tsunami, particularly in terms of wave celerity (speed) and the shape of the free-surface water profiles.

Acoustic-type wave gauges (WG) from the Banner S18U series, capable of sensing water surface elevations within a range of 30-300 mm, were employed to measure water surface elevations in the flume. To measure the flow velocity, a propeller-type current meter (CM) manufactured by Kenek was used. All the equipment used in the experiment were synchronized and logged using the MCR (Multi Channel Recorder) TANDD MCR-4V.

The model structure in the experiment had a height (H_d) of 10 cm and featured identical seaward and landward slopes with an angle of 45 degrees ($\theta = 45°$). The sand box used for the experiment had dimensions of 50 cm in length and 40 cm in width. To analyze the scour profiles, a 2D grid system was attached to the glass panel of the sand box. The scour profiles were then plotted using frame-by-frame video image analysis.

3.1.2 Particle Size Distribution (PSD)

To simulate the dry soil condition on the land side of coastal defenses before a tsunami, the initial sediment condition in the experiments was kept dry. In contrast to the sediment used by Jayaratne et al (2016), different types of sediment were employed to obtain further insight and information during the experiments.

Table 3.2 Characteristics of particle size distribution

Sediment samples	Sediment size (d_{50})	Uniformity coefficient (C_u)	Curvature coefficient (C_c)	Sorting coefficient (Z)
Sediment 1	0.3 mm	1.50	0.78	1.51
Sediment 2	1.13 mm	1.33	0.96	1.14
Sediment 3	2.56 mm	1.95	0.77	1.43
Jayaratne sample	0.36 mm	2.08	0.81	1.57
Ishinomaki city	0.65 mm	2.11	1.10	1.30
Soma city	0.22 mm	1.97	0.98	1.38
Watari city	0.84 mm	6.44	0.67	2.38
Iwanuma city	0.66 mm	2.94	0.87	1.90
Yamamoto city	0.69 mm	6.36	0.75	2.60

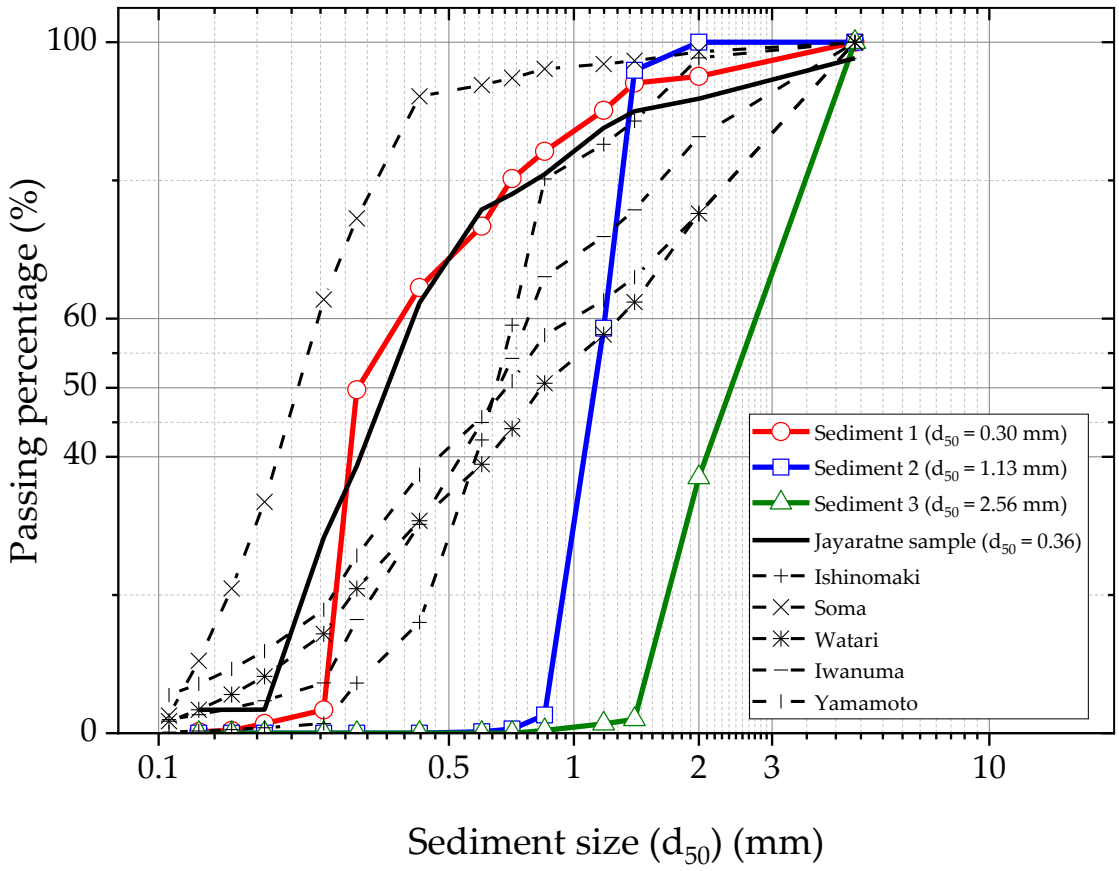

Figure 3.2 Particle size distribution of sediment

(**a**) (**b**) (**c**)

Figure 3.3 a) Sediment 1 (d_{50}= 0.3 mm); b) sediment 2 (d_{50}= 1.13 mm); c) sediment 3 (d_{50}= 2.56 mm)

The particle size distribution of the sediment used in the experiments and additional details can be found in **Table 3.1, Figure 3.2**, and **Figure 3.3**. Sediment 1 had a finer particle size, with a median grain size (d_{50}) of 0.30 mm. Sediment 2 and Sediment 3 were coarser, with median grain sizes (d_{50}) of 1.13 mm and 2.56 mm respectively. It is worth noting that Jayaratne et al (2016) used a sediment with a median grain size (d_{50}) of approximately 0.36 mm in their experiments. This sediment range is commonly associated with granular sands and typically consists of non-cohesive soil particles that do not adhere to each other.

Uniformity coefficient (C_u) and curvature coefficient (C_c) are defined by the following formulas:

$$C_u = \frac{d_{60}}{d_{10}} \tag{3-1}$$

$$C_c = \frac{{d_{30}}^2}{d_{60} x d_{10}} \tag{3-2}$$

Based on the criteria for well-graded sediment, which states that C_u should be greater than 4 for gravel and 6 for sand, and C_c should be between 1 and 3, it can be concluded that the field sample predominantly consists of poorly graded sediment. In particular, the C_u values for the samples in Watari and Yamamoto cities are slightly greater than 6 for sand, but their Cc values are lower than 1 (as shown in **Table 3.1**). On the other hand, the Cc value for the sample in Ishinomaki City is greater than 1, but the C_u value is only 2.11. These findings further support the classification of the sediment in these locations as predominantly poorly graded sediment.

The coefficient of curvature (Z) is calculated using the following formula:

$$Z = \frac{(d_{30})^2}{d_{60} \times d_{10}} \tag{3-3}$$

where all sample's Z values were less than 1, this was also affirmed the uniformly (poorly) graded soil (a well-graded soil has a Z value between 1 and 3).

3.1.3 Structural porosity investigation

To determine the porosity of the model structures, a gravimetric measurement method was employed. This method involves measuring the volume of the pores within the material by filling them with water. Multiple repetitions of the measurement were conducted for each sample stone, and the results were averaged to ensure reliable and accurate findings.

To conduct a gravimetric analysis of coastal structural porosity, the following steps can be followed:

1. Place a sample stone in a measurement glass or container and note its initial weight.

2. Add a known volume of water to the container, ensuring that the sample stone is fully submerged.
3. Allow the water to flow through the sample stone for a specific period, ensuring a consistent flow rate.
4. After the designated time has passed, carefully remove the sample stone from the container and allow it to drain excess water.
5. Weight the sample stone again to determine its final weight.
6. Calculate the weight of the water that passed through the sample stone by subtracting the final weight of the sample stone from its initial weight.
7. Calculate the porosity of the structure by dividing the weight of the water that passed through the sample by the volume of the sample stone.
8. Express the porosity as a percentage by multiplying the calculated value by 100.

Note: It is important to ensure accurate measurements and replicate the process for multiple sample stones to obtain reliable results.

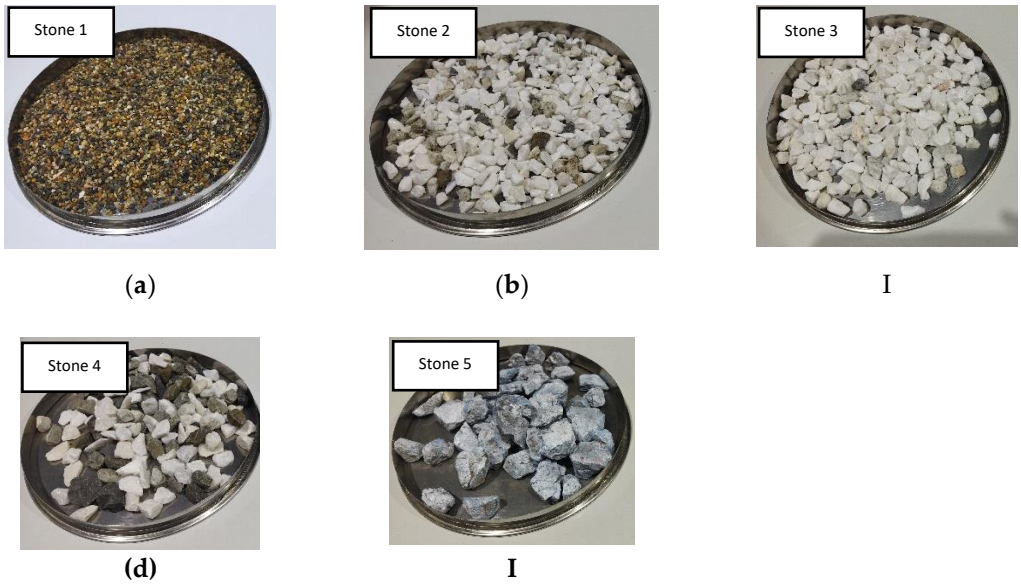

Figure 3.4 a) Stone 1 (D= 2.56 mm); b) stone 2 (D= 4 mm); c) stone 3 (D= 8 mm); d) stone 4 (D= 11.2 mm); e) stone 5 (D= 20 mm)

3.1.4 Laboratory scaling

Buckingham Pi theory, also known as the π theorem or dimensional analysis, is a powerful tool used in engineering and physics to analyze and predict the behavior of physical systems. It is particularly useful in laboratory scaling, where experiments are conducted on a smaller scale to represent larger or more complex systems.

The Buckingham Pi theorem states that if there are N variables involved in a physical phenomenon and these variables can be expressed in terms of k fundamental dimensions, then the relationship between the variables can be described by N - k dimensionless quantities. These dimensionless quantities are known as Pi terms or Buckingham Pi groups. Overall, Buckingham Pi theory and dimensional analysis play a crucial role in laboratory scaling, enabling researchers to study complex systems in a controlled environment and make valuable insights into the behavior of real-world phenomena.

$$D_s = f(D_s, \rho, g, H_d, P_{om}, d_{50}, n) \quad (3\text{-}4)$$

$$\frac{D_s}{H_d} = f(\frac{\rho g H_d}{P_{om}}, \frac{H_d}{d_{50}}, n) \quad (3\text{-}5)$$

Scour depth (D_s) is relevant to some variables including water density (ρ), gravity acceleration (g), dike height (H_d), wave overflowing pressure (P_{om}), median sediment size (d_{50}), and structural porosity (n). Some dimensionless variables can be produced in relation of every related variables to the scour depth, which are relative scour depth ($\frac{D_s}{H_d}$), relative overflowing pressure ($\frac{\rho g H_d}{P_{om}}$), structural and sediment size ratio ($\frac{H_d}{d_{50}}$), and structural porosity (n). Total relevant variables include $D_s, \rho, g, H_d, P_{om}, d_{50}$, and n, hence N= 7. The fundamental dimensions include mass (m), space (L), and time (t), hence N= 3. Therefore, the required nondimensional variables (p) must be 4 (N-k= 7-3= 4), which are $\frac{D_s}{H_d}$, $\frac{\rho g H_d}{P_{om}}$, $\frac{H_d}{d_{50}}$, and n.

Existing predictive equation (eq. 1-1) was proposed based on the relationship of relative scour depth ($\frac{D_s}{H_d}$) and relative overflowing pressure ($\frac{\rho g H_d}{P_{om}}$) through a set of laboratory experiment (Jayaratne et al, 2016). The structure and sediment size ratio ($\frac{H_d}{d_{50}}$) were also proposed by Crowley et al (2020) and Lee and Sturm (2009) to investigate the effect of sediment size (d_{50}) to scour profiles. In this study, this dimensionless variable is adopted and will be presented in Chapter 4. The dimensionless variable of structural porosity (n) will be added to examine the effect structural porosity to scour profiles and will be presented in Chapter 6.

In the experimental setup, dimensional scaling was achieved by applying the principles of the Froude law. The Froude number (F_r) was used to ensure similarity between the prototype in the field (subscript p) and the model in the laboratory (subscript m). The Froude number represents the ratio of inertia forces to gravity forces and is required to be the same for both the prototype and the model. This ensures that the dynamics and behavior of the scaled model accurately represent the prototype conditions in the field.

$$Fr_m = Fr_p = \frac{V_m}{\sqrt{g l_m}} = \frac{V_p}{\sqrt{g l_p}} \tag{3-6}$$

$$V_m = V_p \left[\frac{l_m}{l_p}\right]^{\frac{1}{2}} \tag{3-7}$$

The chosen scale $\left(\frac{l_m}{l_p}\right)$ of 1:50 for the experiment was based on the considerations of the geometry of field tsunami structural defenses in the Tohoku area and the dimensions of the flume. To represent the 5-meter height of the actual structures, a structure height of 10 cm was used in the laboratory.

For the stones used in the experiment, their diameters were scaled down accordingly. Stone 1 with a diameter of 2.56 mm represented a stone size of 0.128 m, stone 2 with a diameter of 4 mm represented a stone size of 0.2 m, stone 3 with a diameter of 8 mm represented a stone size of 0.4 m, stone 4 with a diameter of 11.2 mm represented a stone size of 0.56 m, and stone 5 with a diameter of 20 mm represented a stone size of 0.8 m. These scaled dimensions were chosen to accurately depict the properties of the constructed coastal structures in the Tohoku area (as described by Jayaratne, 2016) and other relevant locations (as described by Juhl, 1995).

Note that the moveable bed area (scour medium) was designed as distorted model which assuming the field sediment size was not scaled. Hence, potential scale effect might slightly influence the result.

3.2 Numerical modeling

3.2.1 Numerical setup

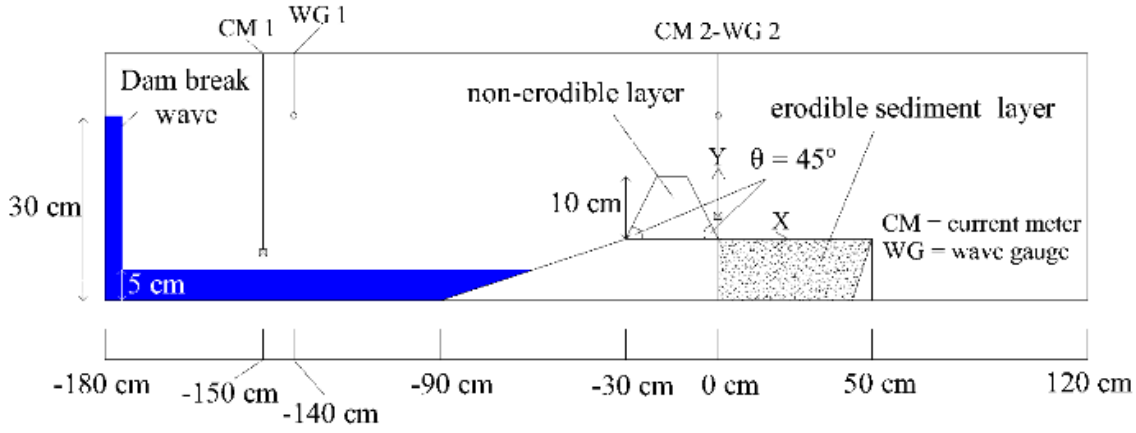

Figure 3.5 Domain configuration used in the XBeach model

Figure 3.5 shows the sketch of the numerical setup where the origin of x-y coordinate is located at the structural toe. In the experiment, a simulation of a dam break wave mechanism was conducted. The offshore boundary of the model was set with a water level of 30 cm. To indicate the location, a specific grid-depth file was utilized. Additionally, an initial water level of 5 cm was imposed in front of the structure, following the experimental condition. A structured grid with a uniform spacing of 1 cm was employed throughout the simulation domain. The simulation was concluded at 19 seconds, as per the experimental suggestion.

In the experiment, the slope and impermeable structure system was treated as a non-erodible layer, while the scour medium system was considered as an erodible sediment layer. The sediment thickness of 10 cm was incorporated into the grid-depth file to represent the scour medium. To prevent reflection from the edge-boundary, an additional length of 70 cm was added to the model setup. This extra length helps to mitigate any unwanted reflections that could interfere with the accuracy of the experiment.

Table 3.3 Setup used in the XBeach model

Caller Function	Value	Note
d_{50}	0.3 mm	Median sediment size 1
	1.13 mm	Median sediment size 2
	2.56 mm	Median sediment size 3
Font	Abs_2d	Absorbing generating weakly reflective boundary used as a 1D inflow boundary
Back	Abs_2d	
Left	Wall	Impermeable wall is a lateral flow boundary
Right	Wall	
Form	Soulsby_vanrijn	Sediment transport formula based on van Rijn III, 2007
	Vanthiel_vanrijn	Sediment transport formula based on van Rijn I and II, 2007
	Vanrijn1993	Sediment transport formula based on van Rijn, 1984
Zs0	30 cm	Initial water at offshore boundary
Morfacopt	0	Morphological acceleration is not considered
Dilatancy	0/1 (0 is default)	Activating function of soil dilatancy effect
Pormax	0.3-0.6 (activated when dilatancy effect is considered)	Max porosity used in the expression of van rhee

Table 3.2 presents the Xbeach model setup, which includes the specifications for the sediment sizes used in the laboratory experiment. The three tested sediment sizes ranged

from fine to coarser sand, with respective d_{50} values of 0.3 mm for sediment 1, 1.13 mm for sediment 2, and 2.56 mm for sediment 3.

In the model setup, the morphological process was considered to have the same time scale as the hydrodynamics process. The soil dilatancy effect was examined by activating the caller function 'dilatancy' and testing various porosity values in the sheared zone (n_l) within the van Rhee expression. This allowed for a more comprehensive exploration of the soil dilatancy effect and its influence on the overall system behavior.

3.2.2 Numerical validation

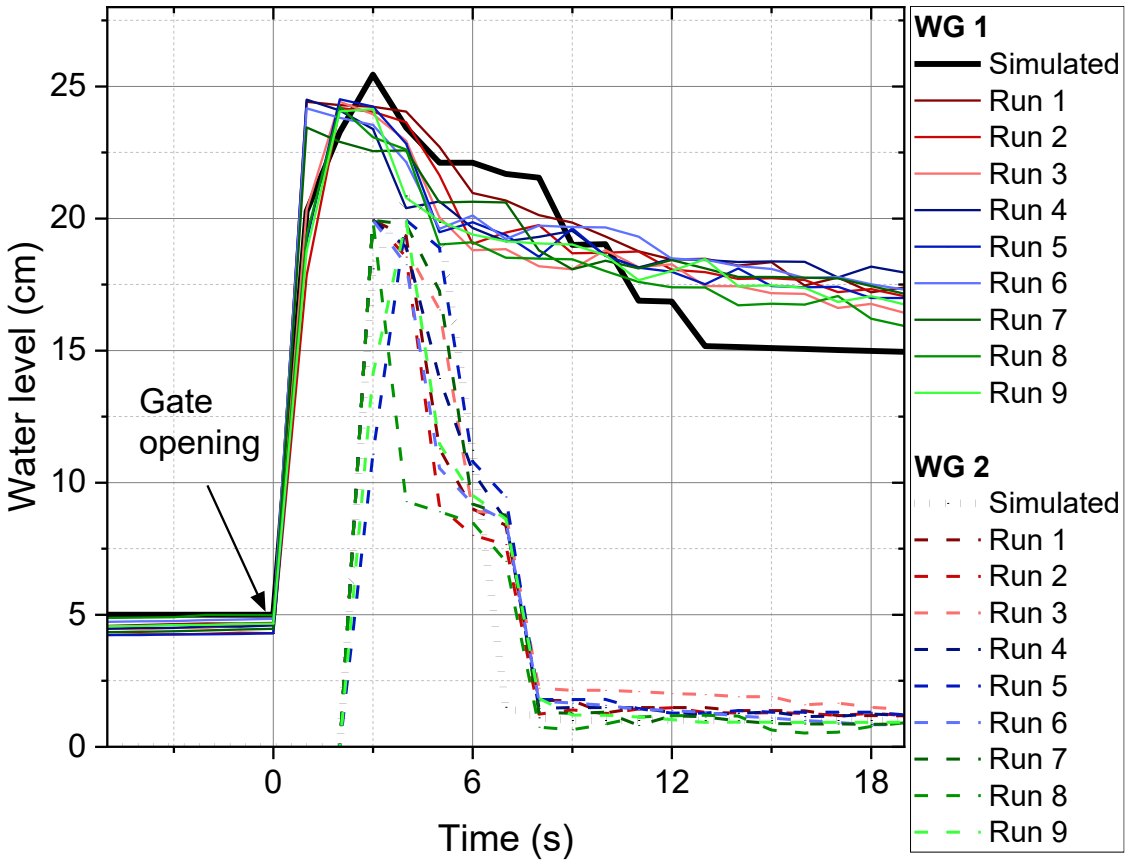

Figure 3.6 Simulated water level variation compared to experiments

The performance of the Xbeach simulation was assessed by comparing the simulated water flow with data from two wave gauges (WGs) and one propeller-type current meter (CM) used in the experiment (**Figure 3.6**). Due to apparatus limitations, the second CM was not utilized during the simulation to monitor incoming velocity reaching the erodible sediment layer; it was used afterward for analysis.

The simulated wave heights aligned with the measured wave heights at WG1 (located at x = -140 cm) and WG2 (located at x = 0 cm). Figure 3.6 illustrates the comparison between

the simulated water level and the experimental data, encompassing nine runs with three repetitions for each sediment size. Overall, Xbeach demonstrated the capability to model the variation of water level at both wave gauges, indicating its effectiveness in simulating the dam break wave mechanism.

Chapter 4

Sediment Size Effects

4. Sediment Size Effects

4.1 Flume hydrodynamics

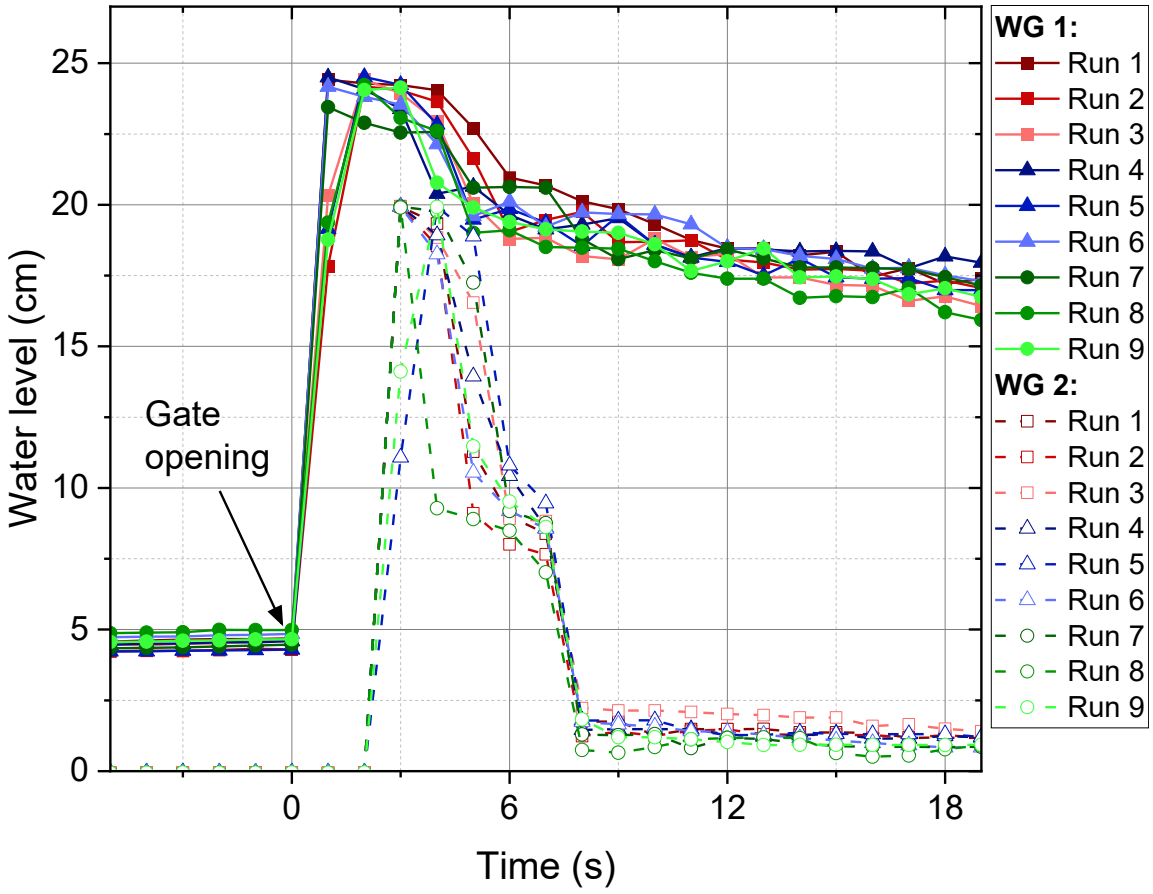

Figure 4.1 Variation of water level in the flume

In the experimental setup, the initial conditions were carefully controlled to ensure repeatability and reproducibility of the tests. For each sediment size, three test runs were conducted. Test runs 1-3 were conducted for sediment 1 (d_{50} = 0.3 mm), runs 4-6 for sediment 2 (d_{50} = 1.13 mm), and runs 7-9 for sediment 3 (d_{50} = 2.56 mm).

Figure 4.1 illustrates the variation of water levels at two locations in the flume, namely WG1 and WG2, for each test run. The initial water volume was accumulated behind a lifting

gate until it reached a water depth of 30 cm. An initial water depth of approximately 5 cm was set upstream (WG1, x = -140 cm) on the seaward side of the structure for all experiments.

From WG2 (x = 0 cm, landside edge of the structure), an average water depth of approximately 20 cm was generated, which was then considered as the inundation depth (h). The gate was closed shortly after the first wave was generated to examine the effect of the first tsunami wave in all experiments.

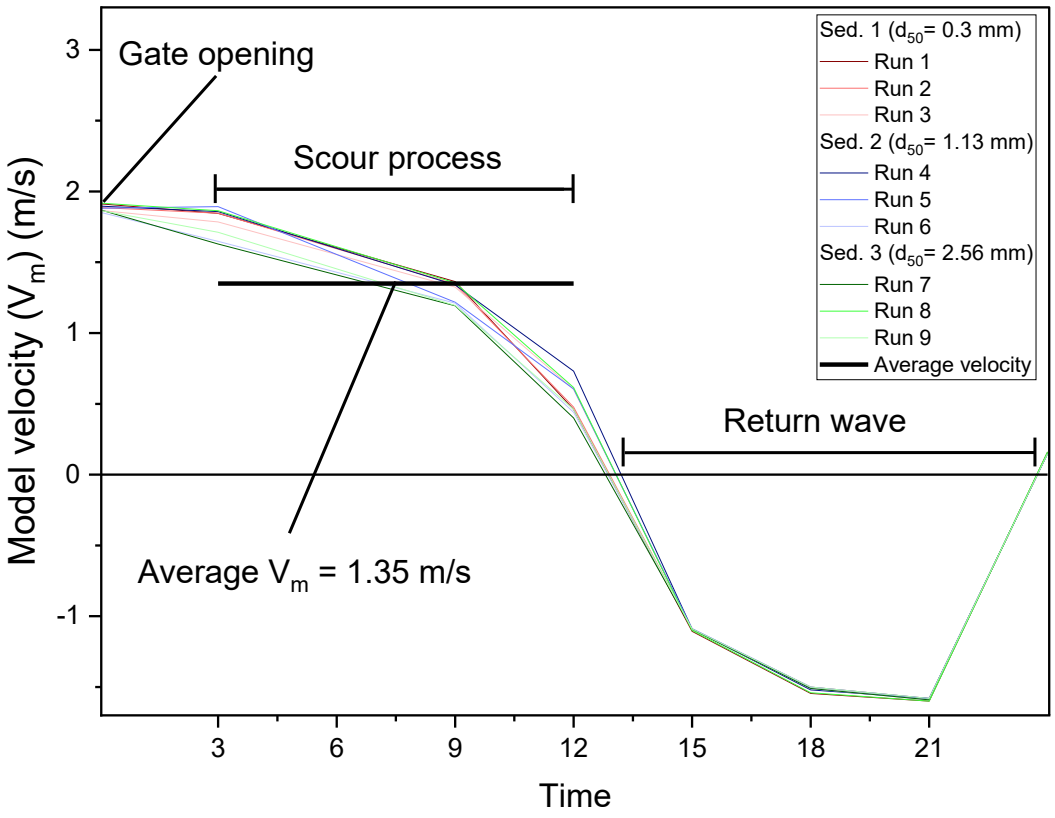

Figure 4.2 Velocity profile of the flume

From **Table 2.1**, the field data (V_p) were in the range of 8.97 to 10.36 m/s. By applying eq. 3-7, velocity in the laboratory (V_m) needs to be in the range 1.27 to 1.46 m/s. **Figure 4.2** shows the velocity profile measured in the laboratory where some moments are showed, since the gate opening, scour process, and the return waves (minus values). The averaged measured velocity in the laboratory (C_m, x = -150 cm) during the scour process is 1.35 m/s (black line) which is in line with the requirements of kinematic similitude for laboratory scaling.

4.2 Scour process

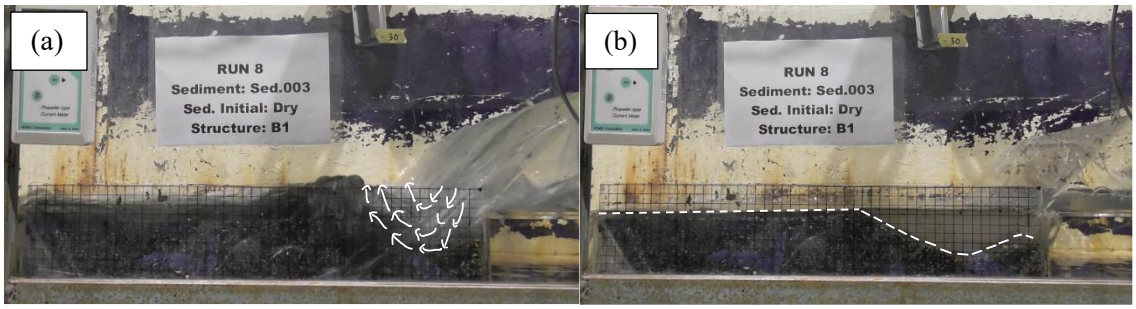

Figure 4.3 Landward coastal structure scour: (a) steady streaming process, (b) the equilibrium development scour profile

The main mechanism of coastal structure scour observed in the experiments is the steady-streaming process, which is responsible for the formation of scour holes. This process involves a vortex flow within the sediment mass, acting as a digger of the scour hole. Similar steady-streaming processes have been observed in the case of seaward scour holes around rubble mound breakwaters and in the 2018 Palu tsunami.

Figure 4.3 illustrates the development of landward toe scour in the experiments. The steady-streaming process is indicated by the white arrows in **Figure 4.3a**, highlighting the capture of sediment by the vortex flow. **Figure 4.3b** shows the equilibrium state of the final scour profile, which will be analyzed for predictions of scour depth and extent.

4.3 Observed scour profiles

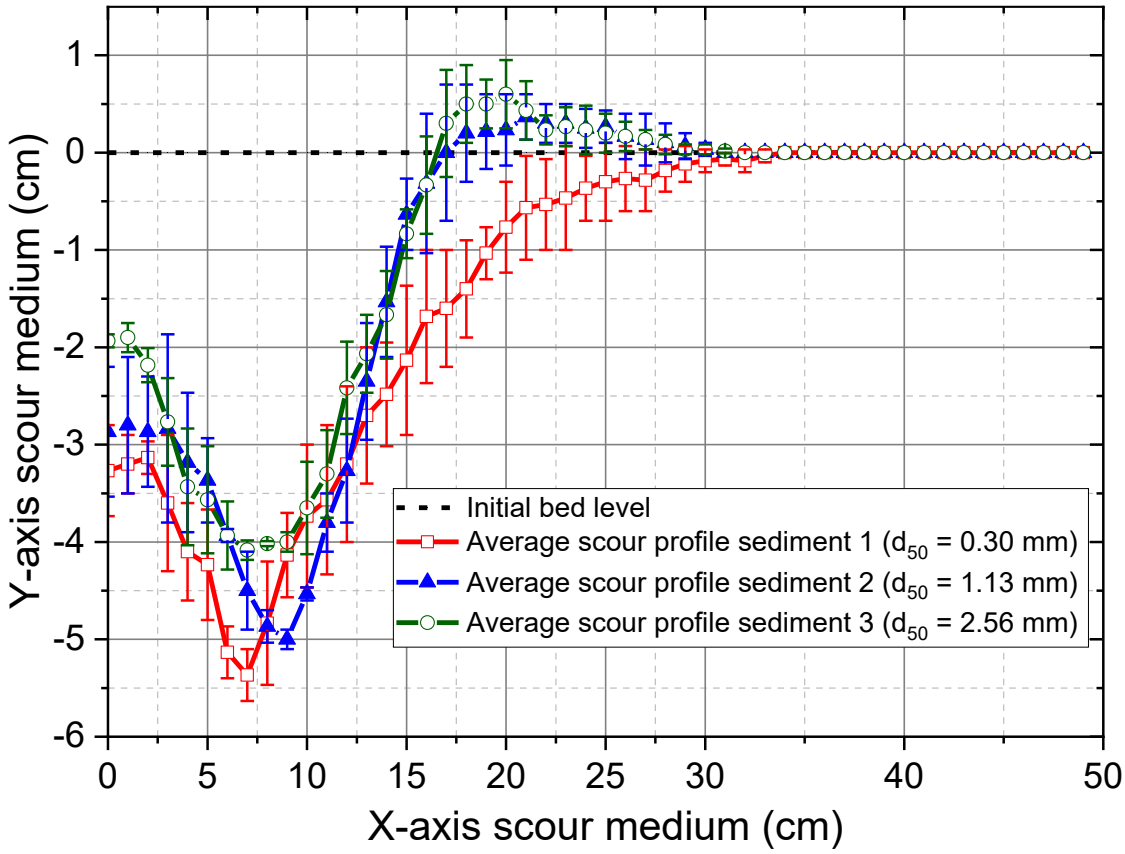

Figure 4.4 Measured scour profiles with error bars

Figure 4.4 illustrates the average scour depths and their deviations (errors) from the mean for each sediment size, along with the observed scour patterns for three test runs. The variability in the observed scour patterns can be seen.

For sediments 2 (d_{50} = 1.13 mm) and 3 (d_{50} = 2.56 mm), both erosion and deposition patterns can be identified in the scour regime. However, for sediment 1 (d_{50} = 0.30 mm), only erosion is observed, and there is no significant deposition. The erosion volumes are noticeably higher than the deposition volumes for sediments 2 and 3, indicating that the remaining eroded sediment is flushed out of the sediment region.

Table 4.1 Experimental conditions and measured parameters

Run No.	d_{50} (mm)	h (cm)	V_m (cm/s)	D_s (cm)	L_s (cm)
1	Sed. 1 = 0.30	19.92	139.5	5.6	34
2		19.94	138.9	5.4	29
3		19.94	139.4	5.4	33
4	Sed. 2 = 1.13	19.94	145.6	4.9	19

5		19.93	149.9	5.1	15.5
6		19.92	128.8	5.0	18
7	Sed. 3 = 2.56	19.93	127.3	4.1	16.5
8		19.90	143.8	4.2	17.5
9		19.90	125.8	4.3	15.5

In the case of sediment 1, the force of the overflowing wave is likely energetic enough to transport the finer sediment towards the land side of the structure, resulting in the absence of deposition patterns. More details about the sediment conditions used and the corresponding observed parameters for each test run can be found in **Table 4.1**.

4.4 improved predictive equation

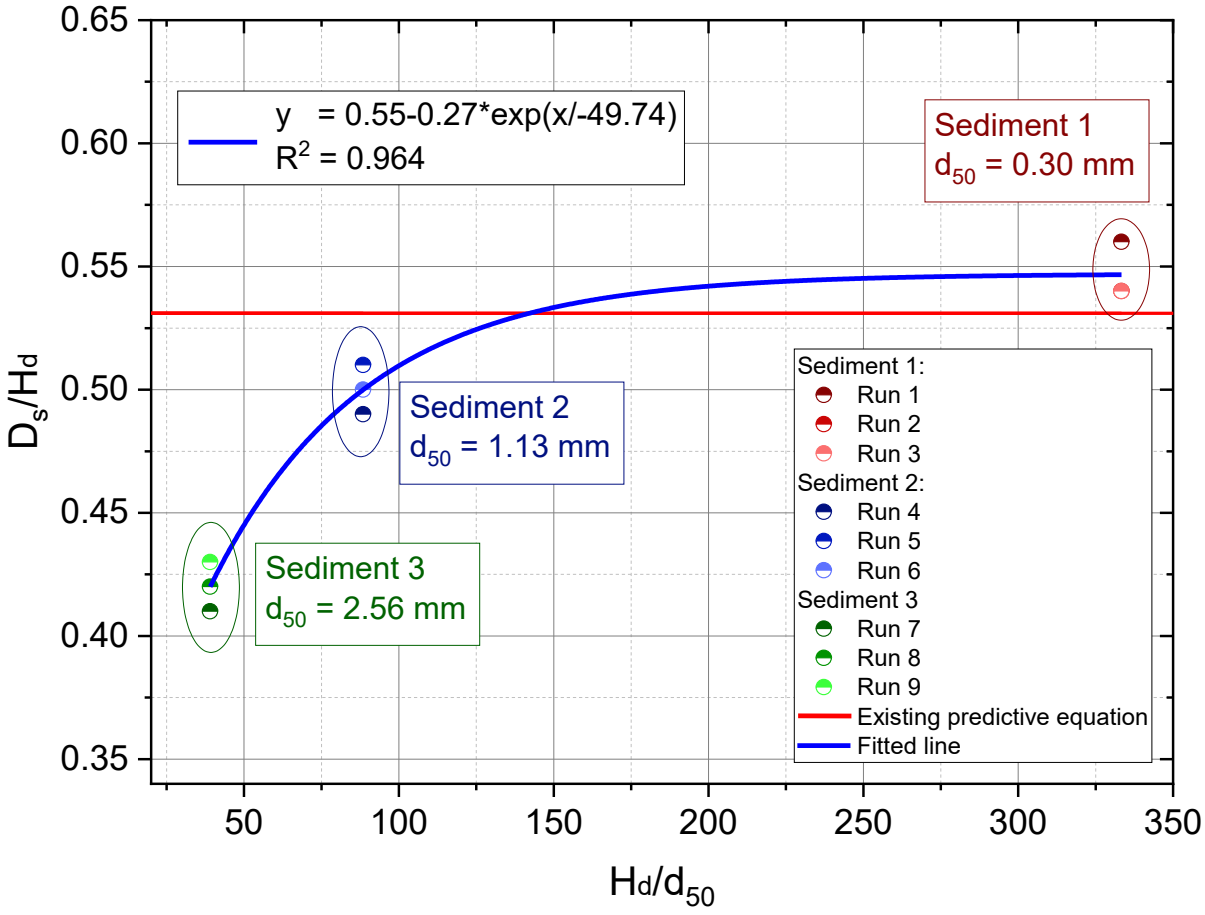

Figure 4.5 Relationship between relative scour depth (D_s/H_d) and structure height/sediment size (H_d/d_{50})

Figure 4.5 shows the relationship between relative scour depth (D_s/H_d) and the ratio of structure height to sediment size (H_d/d_{50}). The blue line represents the correlation between D_s/H_d and H_d/d_{50}, which follows an exponential equation with a coefficient of determination (R^2) of 0.964.

The general trend observed is that as the sediment size becomes coarser (lower H_d/d_{50}), the scour depth decreases, and vice versa, within the range of tested sediment sizes. Additionally, the red line represents the linear trendline of the existing predictive equation plotted using Eq. 1. This line indicates that the existing equation can only predict a single value of scour depth in the current setup, regardless of the sediment sizes in the bed. Overall, the exponential correlation provides a better fit to the data and demonstrates the influence of sediment size on the relative scour depth, indicating the limitations of the existing linear predictive equation.

Based on the observations from Figure 4.4, where the sediment size effect deviates from the existing equation result, it is possible to normalize the fitted line of observed relative scour depths (D_{so}/H_{do}) to the predicted value (D_{sp}/H_{dp}). This normalization can be achieved by introducing a new fitted coefficient (λ_s) as a function of d_{50}.

$$\lambda_s = \frac{[\frac{D_{so}}{H_{do}}]}{[\frac{D_{sp}}{H_{dp}}]} \tag{4-1}$$

Based on the provided information, the observed relative scour depth (D_{so}/H_{do}) follows the trendline $0.55\text{-}0.27\times\exp(\text{-}H_d/(49.74\times d_{50}))$. In the current experimental setup with a coastal structure height (H_d) of 20 cm, inundation depth (h) of 10 cm, and dike slope (θ) of 45 degrees, setting up λ as 1, and applying these values to the existing predictive equation, the predicted relative scour depth (D_{sp}/H_{dp}) is 0.62.

Inputting the relevant values in the above equation to the following equation, we will draw the updated fitted coefficient (λ_s) as a function of median sediment size (d_{50}).

$$\lambda_s = \frac{0.55 - 0.27 \times \exp\left(-\frac{H_d}{49.74 \times d_{50}}\right)}{0.62} \tag{4-2}$$

$$\lambda_s = 0.89 - 0.44 \times \exp\left(-\frac{H_d}{49.74 \times d_{50}}\right) \tag{4-3}$$

$$\frac{D_s}{H_d} = \lambda_s \times \exp\left(-\frac{\sqrt{H_d}}{2.5\sqrt{h}\sin\theta}\right) \tag{4-4}$$

Based on the information provided, the coefficient λ_s can be applied to the updated predictive equation to improve its accuracy (**Figure 4.6**). The updated equation would follow

the best-fit line of the overall experimental dataset for sediment sizes within the range of d_{50} = 0.30 - 2.56 mm.

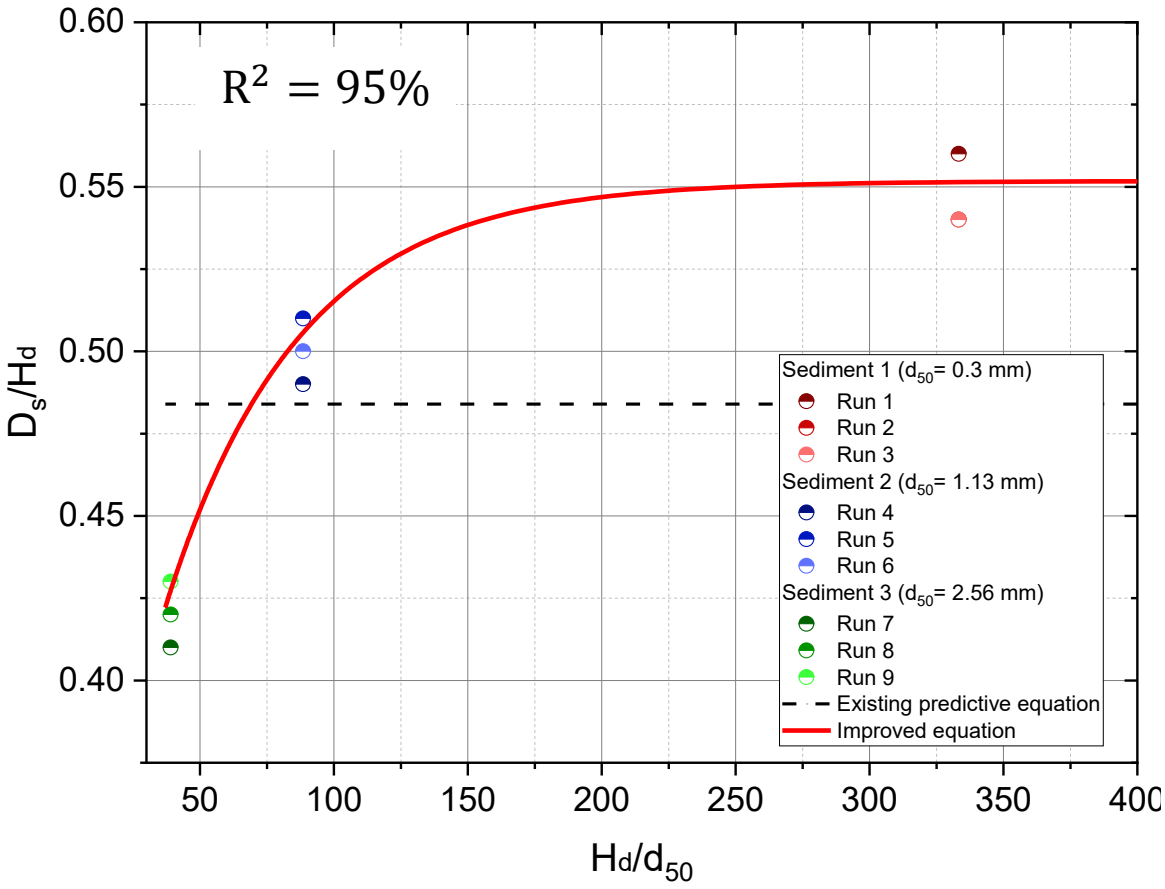

Figure 4.6 Validation check of the improved predictive equation to the experimental data

However, it is important to note that for sediment sizes (d_{50}) lower than 0.30 mm, special consideration is required due to the cohesive nature of the sediment when mixed with water. The behavior of such sediments may differ from the observed trends in the laboratory, and therefore, caution should be exercised when applying the predictive equation in those cases.

4.5 Conclusion

The small-scale laboratory experiments conducted in this study have highlighted the importance of considering the sediment size effect on landward coastal structure toe scour. The existing predictive depth equation proposed by Jayaratne et al (2016). did not explicitly account for this effect and provided a single value of relative scour depth regardless of the sediment size.

Through the laboratory investigation, it was observed that there is a correlation between the median sediment size (d_{50}) and the predicted scour depth, following an exponential

relationship. By normalizing the fitted coefficient (λ) in the existing equation to produce the updated fitted coefficient (λ_s) as a function of d_{50}, the updated predictive equation incorporates the sediment size effect and improves its performance in predicting scour depths.

It is worth noting that this study focuses on one aspect of the uncertainties associated with the existing practical predictive depth equation. Factors such as geotechnical properties, structural integrity, and flow hydrodynamics variability of the landward coastal structure toe scour should also be considered for a comprehensive understanding. Additionally, conducting experiments at a larger geometrical scale is recommended to minimize the scale effects and further improve the predictive capabilities of the equation.

Chapter 5

Numerical Investigation (XBeach)

5. Numerical Investigation (XBeach)

5.1 Sensitivity to transport formulas

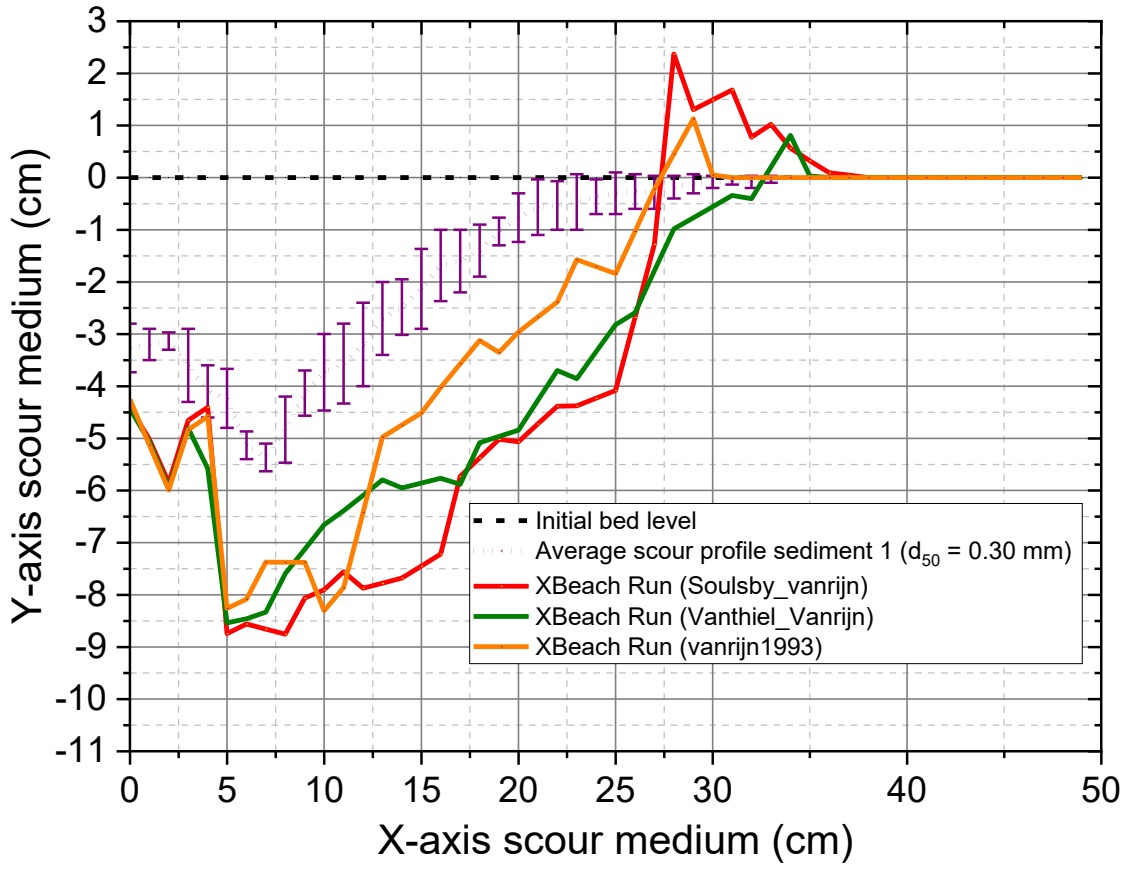

Figure 5.1 Sensitivity to developed scour profiles for each sediment transport formula

The adjustment of hydrodynamics-induced sediment transport coefficients, such as facua (calibration factor for time-averaged flows due to wave skewness and asymmetry) and facSk (factor for bed slope effect), as suggested by McCall et al (2010). and Elsayed and Oumeraci (2017), did not have an impact on the results of the simulation. These coefficients are believed to have minimal influence on the fast and short landward scour phenomenon observed in the laboratory model.

In **Figure 5.1**, the developed scour profile for three different sediment transport equations is presented. The average scour profile from the experiment for sediment 1 (with d_{50}= 0.3 mm) is represented by a dashed line with error bars. The default transport formula used in the simulation is vanthiel-vanrijn.

Upon evaluation, it is observed that the choice of sediment transport formula significantly affects the model's prediction of the scour profile for sediment 1. Among the tested formulations, vanrijn1993 shows better agreement with the experimental results, particularly in terms of the maximum scour depth location and the subsequent scour profile. The values predicted by this formula are closer to the experimental data. Therefore, for the subsequent analysis, vanrijn1993 will be used as the preferred sediment transport formulation.

5.2 Froude number

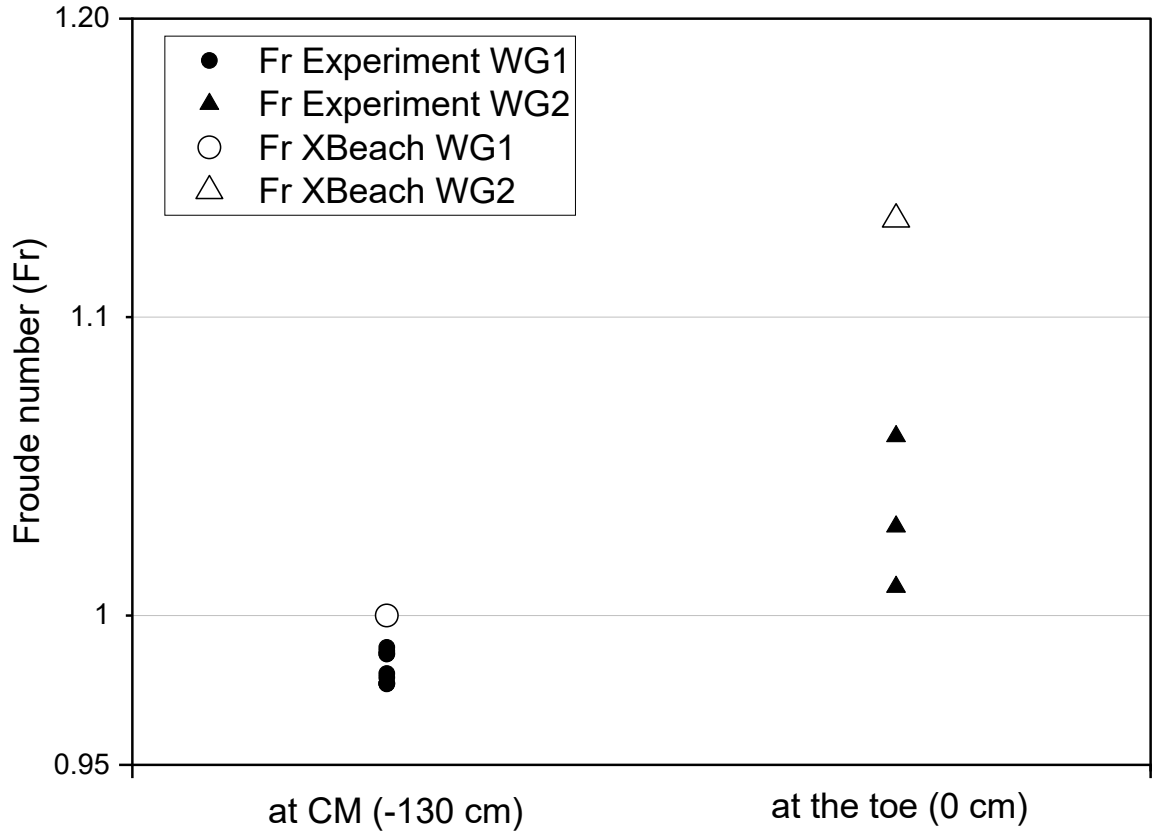

Figure 5.2 Simulated Froude number compared to experiments in WG1 and WG2

Figure 5.2 demonstrates the evaluation of simulated velocity, represented by the Froude number $\left(Fr = \frac{V_{max}}{\sqrt{gH_d}}\right)$, in comparison to the measured data obtained from the laboratory experiment. The measurements were taken at two locations: CM1, located at x = -150 cm,

and CM2, located at the toe (x = 0 cm). Due to instrument limitations, the data at CM2 was collected separately with three repetitions.

The evaluation reveals that the simulated maximum flow velocity (V_{max}) generally exceeded the measured values in the laboratory experiment. Specifically, at the toe location (X = 0 cm), the simulated flow velocity exceeded the measured values by up to 13%. It is important to note that the velocity calculated by XBeach is a depth-averaged value, which may contribute to the differences observed between the simulated and measured velocities. This presumably contributes to the overestimation of the simulated scour profiles.

5.3 Hindered erosion by soil dilatancy

Under high-flow velocity conditions and significant water level changes, the phenomenon of dilatancy may impede sediment pick up and transport, thereby slowing down the rate of erosion. To address this effect, van Rhee proposed an adjustment to the critical shield parameter ($\theta_{cr}^{adjusted}$). The adjusted parameter considers the impact of dilatancy and provides a more accurate representation of the sediment behavior under such conditions.

$$\theta_{cr}^{adjusted} = \theta_{cr}\left(1 + \frac{v_e}{k_l}\frac{n_l - n_0}{1 - n_l}\frac{A}{\Delta}\right) \quad (5\text{-}1)$$

$$k_l = \frac{g}{160\nu} {D_{15}}^2 \frac{{n_0}^3}{(1 - {n_0}^2)} \quad (5\text{-}2)$$

$$v_e = \begin{cases} -\frac{dz_b}{dt} & if \quad \frac{dz_b}{dt} < 0 \\ 0 & else \end{cases} \quad (5\text{-}3)$$

in which θ_{cr}, k_l, v_e, n_0, n_l, and Δ are shield parameter, permeability, erosion velocity, porosity prior erosion, porosity in the sheared zone (dilated), and relative sediment density respectively. A is considered as van rhee coefficient based on experiment.

The determination of the porosity in a sheared zone (n_l) is challenging due to the intricate particle-stirring process associated with high-velocity flow. In XBeach, the parameter 'pormax' is used as a caller function to specify the dilated porosity value, which can be selected within the range of 0.3 to 0.6. In terms of the critical shield parameter (θ_{cr}) and critical flow velocity (U_{cr}), Elsayed and Oumeraci proposed the following relationship:

$${U_{cr}}^2 = \theta_{cr}\frac{g d_{50}(s - 1)}{C_f} \quad (5\text{-}4)$$

in which U_{cr}, g, s, and c_f are critical velocity, gravity acceleration, relative density (ρ_s/ρ), and roughness coefficient respectively.

The augmentation of the critical Shields parameter in the equation results in an elevated critical velocity needed to initiate sediment particle movement. Consequently, the disparity

between stirring velocity and critical velocity decreases, leading to a reduction in erosion rates. This phenomenon can be attributed to dilatancy, which generates an additional inward force on soil particles, enhancing their resistance to erosion. In a study by De Vet et al (2015), the dilatancy effect was employed to limit erosion artificially in a dune breaching scenario. This approach proved relatively successful in mitigating overestimations obtained from XBeach simulations.

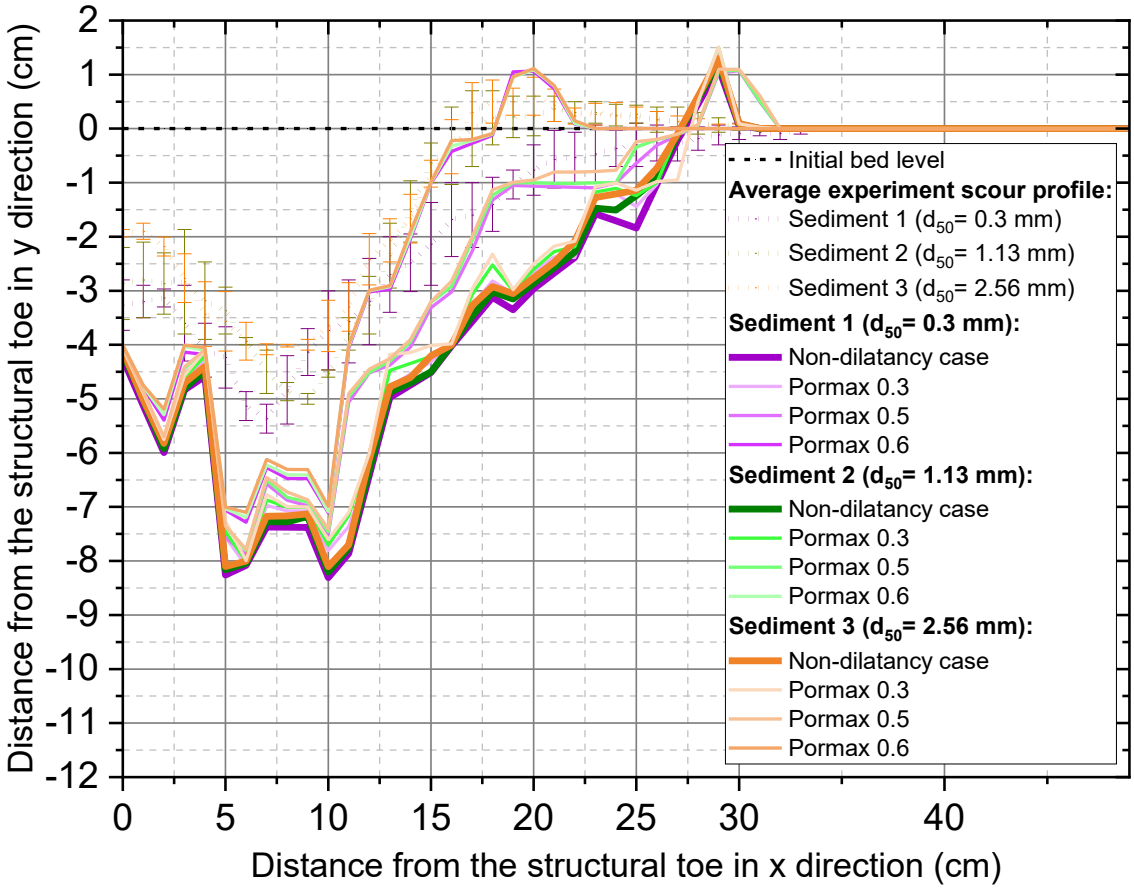

Figure 5.3 Developed scour profiles after applying artificial erosion limiter

In **Figure 5.3**, the scour profiles resulting from different pormax values (0.3, 0.5, and 0.6) are depicted for each sediment size. The dashed lines represent the average scour profiles observed in the experiment. Overall, the landward scours, which correspond to erosion areas, exhibit a similar development, and follow a comparable pattern to the experimental results. However, the simulated scour depth (D_s) still tends to be overestimated. Notably, when the pormax value is increased, the scour profile shows some recovery after reaching the maximum scour depth at x = 5 cm. The subsequent discussion will delve into the evaluation of the landward scour profile and its distinctive characteristics.

5.4 Scour profile validation

The performance of the model in predicting the scour profile, particularly its morphology shape, can be assessed using the Brier Skill Score (BSS). The BSS is calculated using the following formula:

$$BSS = 1 - \left[\frac{\left\{ \frac{\sum_0^n \left(|y_{b,c} - y_{b,m}| - \Delta y_{b,m} \right)^2}{n} \right\}}{\left\{ \frac{\sum_0^n \left(y_{b,0} - y_{b,m} \right)^2}{n} \right\}} \right] \tag{5-5}$$

where n is the number of grids in x direction in the scour medium (Fig. 1). The subscripts c and m refer to the computed (XBeach) and measured (laboratory experiments) scour depths on every position in horizontal axis. $\Delta y_{b,m}$ is error of measured bed level, which is 0.1 m for field conditions and 0.02 m for laboratory conditions.

Table 5.1 BSS score simulation

Sediment size	Dilatancy function conditions		BSS Score	
			Score	Qualification
Sediment 1 (d50= 0.3 mm)	Dilatancy is not activated		0.19	Poor
	Pormax	0.3	0.35	Reasonable/Fair
		0.5	0.71	Good
		0.6	0.78	Good
Sediment 2 (d50= 1.13 mm)	Dilatancy is not activated		-0.88	Bad
	Pormax	0.3	-0.56	Bad
		0.5	0.14	Poor
		0.6	0.76	Good
Sediment 3 (d50= 2.56 mm)	Dilatancy is not activated		-4.92	Bad
	Pormax	0.3	-4.38	Bad
		0.5	-2.72	Bad
		0.6	-1.21	Bad

The Brier Skill Score (BSS) values for each simulation are summarized in **Table 5.1**. For sediment 1 (d_{50}= 0.3 mm), activating the soil dilatancy effect improves the BSS value from a poor qualification (BSS= 0.19) to a good qualification (BSS= 0.78). Similarly, for sediment 2 (d_{50}= 1.13 mm), implementing the erosion limiter effect of dilatancy enhances the BSS value from a bad grade (BSS= -0.88) to a good category (BSS= 0.76). However, for

sediment 3 (d_{50}= 2.56 mm), the implementation of soil dilatancy effect does not improve the BSS value, and the BSS remains below 1 for all pormax values.

In summary, activating the erosion limiter through soil dilatancy (pormax) of 0.6 leads to good agreement based on the BSS evaluation for sediment 1 and 2. However, for coarser sediment (sediment 3, d_{50}= 2.56 mm), soil dilatancy (pormax) does not improve the qualification of the scour profile, although the BSS value increases.

5.5 Evaluation of improved scour features

The evaluation of the improved simulated landward scour, incorporating soil dilatancy (pormax), includes several scour properties such as erosion volume (V_{err}) and scour depth (D_s). The model results, represented by the solid line, will be compared to the experimental results (dashed line) for each sediment size.

By implementing the soil dilatancy effect, the model aims to improve its performance in capturing the erosion characteristics and scour depth. The comparison between the solid line (improved simulation) and the dashed line (experimental data) will provide insights into the effectiveness of incorporating soil dilatancy in predicting the scour properties.

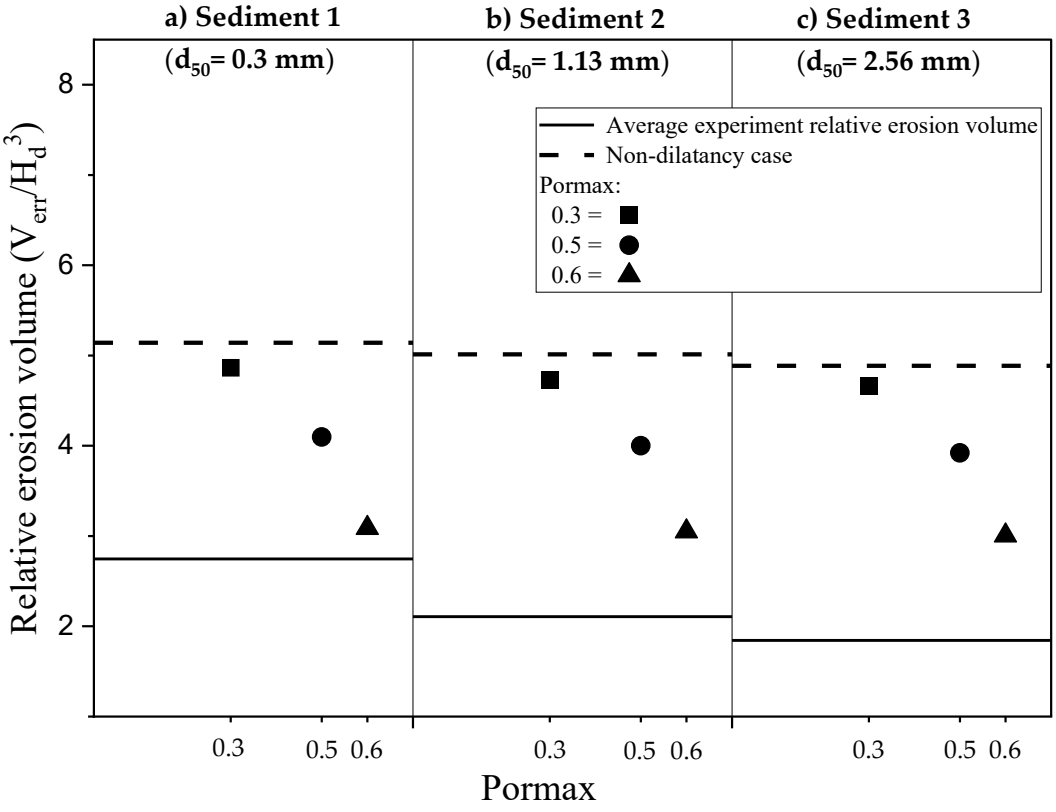

Figure 5.4 Relative erosion volume (V_{err}/H_d^3) evaluation after applying artificial erosion limiter

In **Figure 5.4**, the trend of relative erosion volume (V_{err}/H_d^3) is depicted for different values of pormax (0.3, 0.5, and 0.6). The relative erosion volume represents the erosion volume normalized by the cube of the water depth (H_d) in the laboratory experiment. It can be observed that as the value of pormax increases, approaching 0.6, the relative erosion volume decreases significantly. This suggests that by increasing the critical shear parameter associated with soil dilatancy, the erosion volume in the simulation becomes closer to the erosion volume observed in the laboratory experiment.

The trend shown in Figure 5.4 indicates that implementing a higher pormax value (such as 0.6) can lead to a better agreement between the simulated erosion volume and the laboratory data. This suggests that the soil dilatancy effect has a significant influence on reducing the relative erosion volume in the model.

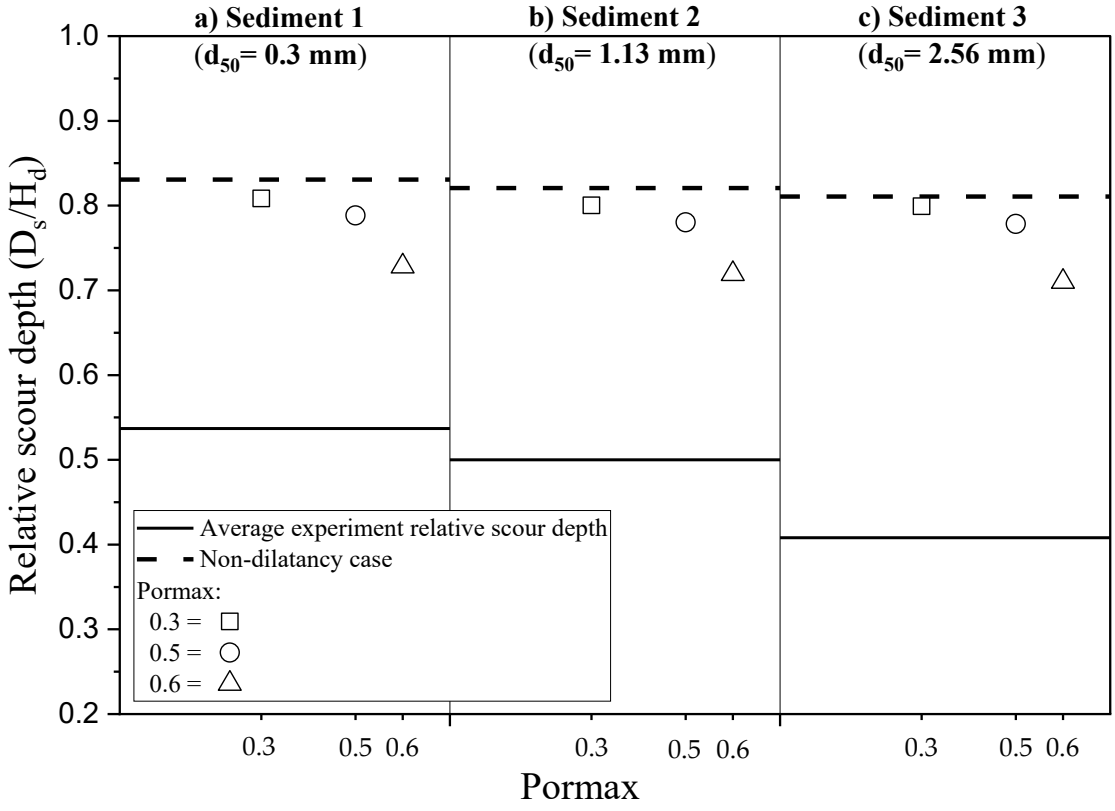

Figure 5.5 Relative scour depth (D_s/H_d) evaluation after applying artificial erosion limiter

In **Figure 5.5**, the relative scour depth (D_s/H_d) patterns are shown for different pormax values. It can be observed that increasing the critical shield parameter (higher pormax) has a limited effect on reducing the relative scour depth. While there is some reduction in the relative scour depth with higher pormax values, the simulated scour depths are still significantly higher than the experimental results. The gap between the simulated and

experimental values suggests that there are other factors or mechanisms influencing the scour depth that are not fully captured by the model, even with the implementation of the soil dilatancy effect.

Therefore, although the higher pormax values show some improvement in reducing the relative scour depth, it is evident that further refinements or adjustments to the model may be necessary to better match the experimental results.

5.6 Bed Shear Stress

Bed shear stress is applied to improve the result of the model. The default shear stress used Chezy formula as follow,

$$C_f = \sqrt{\frac{g}{C^2}} \tag{5-6}$$

Where C_f is friction coefficient (dimensionless) and C and Chezy coefficient. Referring manning formula, friction coefficient is formulated as follow,

$$C_f = \sqrt{\frac{gn^2}{h^{1/3}}} \tag{5-7}$$

Where n is manning coefficient (related to material types) and h is water depth. If C is 55 (default), the C_f will result 0.057 which is basically lower than acrylic board (material used in the laboratory).

Manning coefficient's scenario study is conducted to see the effect bed shear stress as tabled in the following. Case 1 is basically the default value of the model. Case 2-4 the manning coefficient (n) is increased gradually and see the effect to Froude number and scour depths.

Table 5.2 Manning's coefficient scenario study

No	n	C_f
Case 1	C= 55	0.057
Case 2	0.014	0.061
Case 3	0.015	0.065
Case 4	0.016	0.070

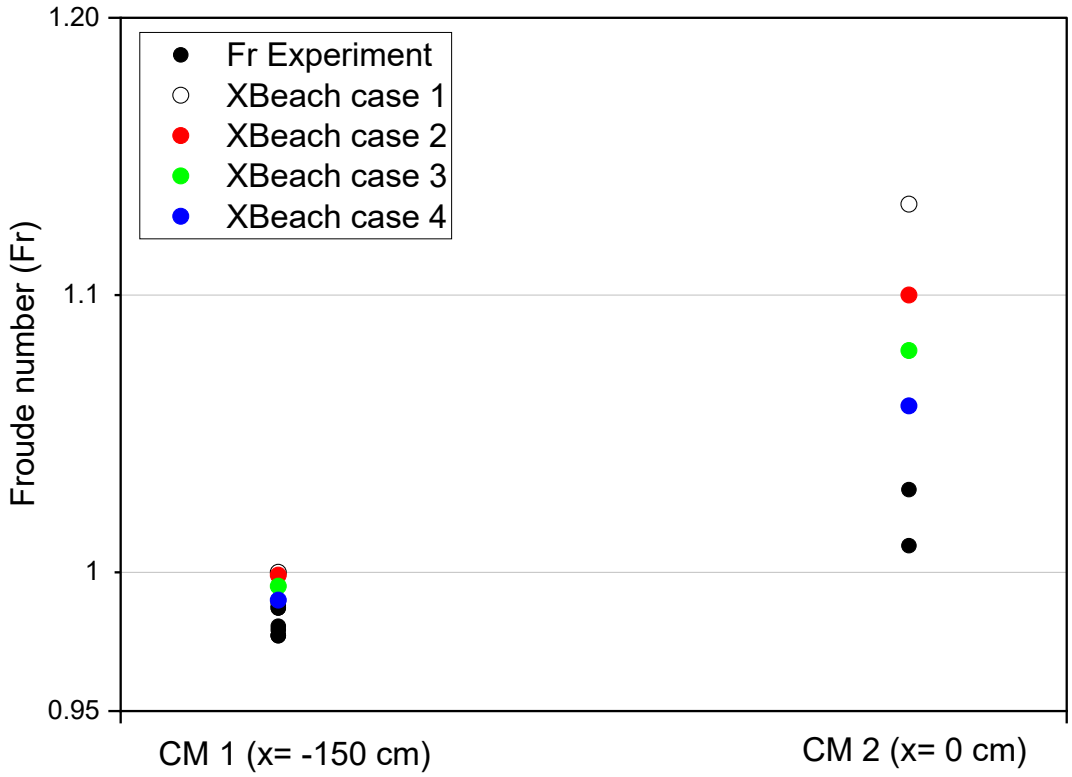

Figure 5.6 Froude number evaluation of increasing bed shear stress

Figure 5.6 shows the evaluation of Froude number (related velocity) of water flow by increasing the effect bed shear stress. Especially in the CM 2 (after flow passing the model structure), the result is improving to the point close to experimental result. The case 4 (n= 0.016) is for asphalt (rough material). The higher than case 4 manning's coefficient is for very rough material surface (stones), therefore we did not test it.

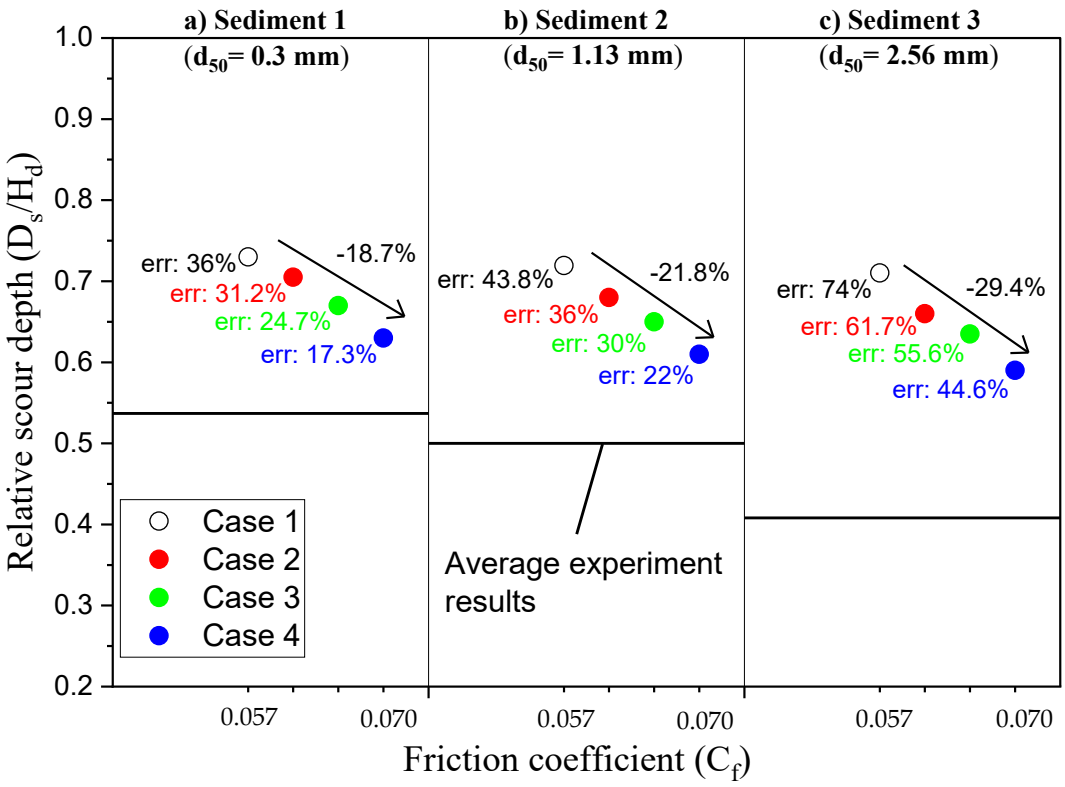

Figure 5.7 Relative scour depth (D_s/H_d) evaluation after applying higher bed shear stress

Figure 5.7 displays the evaluation of relative scour depth after applying higher bed shear stress effects. For every sediment size, we see the improvement of the result (errors to the experimental results decrease). Especially for sediment 1 (d_{50}= 0.3 mm) and 2 (d_{50}= 1.13 mm), the results error for case 4 are now 17.3% and 22% respectively. For sediment 3 (d_{50}= 2.56 mm) the error is reduced from 74% (default number) to 44.6% (case 4).

Overall, applying higher shear stress on the model will improve the result significantly. Although, the scenarios for bed shear stress exceed the theoretical suggestion. Physically, the higher stress can be interpreted as higher energy loss in the laboratory works related water and model structure interaction, loss of water to the edge of structure and scour medium system, etc.

5.7 Conclusion

This chapter focused on simulating the landward scour process using the XBeach model. The model successfully captured the water level changes resulting from the dam-break mechanism. However, it tended to overestimate the morphodynamical aspects, likely due to an overestimation of the simulated flow velocity. To address this issue, the study activated the soil dilatancy effect by increasing the critical shield parameter through higher porosity

in the sheared zone (n_l) or using the pormax function. This adjustment helped improve the agreement between the simulated erosion volume and the experimental results. Adopting higher bed shear stress (manning coefficient) has a good potential to improve results, especially reducing flow velocity in the scour medium and scour depth. In terms of physicality, increased stress can be understood as a greater amount of energy being lost in laboratory activities involving water and interactions with model structures. This includes water loss towards the edges of the structure and within the system of eroding materials.

However, the study also identified limitations in accurately predicting the scour depth (D_s) using the XBeach model. Further improvements are needed to better align the simulated scour depths with the experimental data. In conclusion, this study provides valuable insights into the capabilities and limitations of the XBeach model for simulating landward scour. It highlights the potential of using the soil dilatancy effect to improve the model's performance but also emphasizes the need for ongoing research and refinement in this area.

Chapter 6

Structural Porosity Effects

6. Structural Porosity Effects

6.1 Structural porosity

Coastal structural porosity, or coastal permeability, plays a crucial role in determining the behavior and performance of coastal structures. It refers to the ability of these structures, such as sea walls or breakwaters, to allow water and sediment to pass through them. The porosity of coastal structures can significantly impact the overall health and stability of the surrounding coastal environment, including the processes of sediment transport and scour.

Gravimetric analysis is one method commonly used to measure coastal structural porosity. This technique involves collecting a sample of the structure and analyzing the amount of void space or water that can flow through it. By quantifying the porosity, researchers can gain insights into the structure's permeability and its potential impact on sediment movement.

Table 6.1 Porous structures porosity

Stone samples	Stone size (D)	Average porosity
Stone 1	2.56 mm	36%
Stone 2	4 mm	41%
Stone 3	8 mm	41%
Stone 4	11.2 mm	42%
Stone 5	16 mm	44%

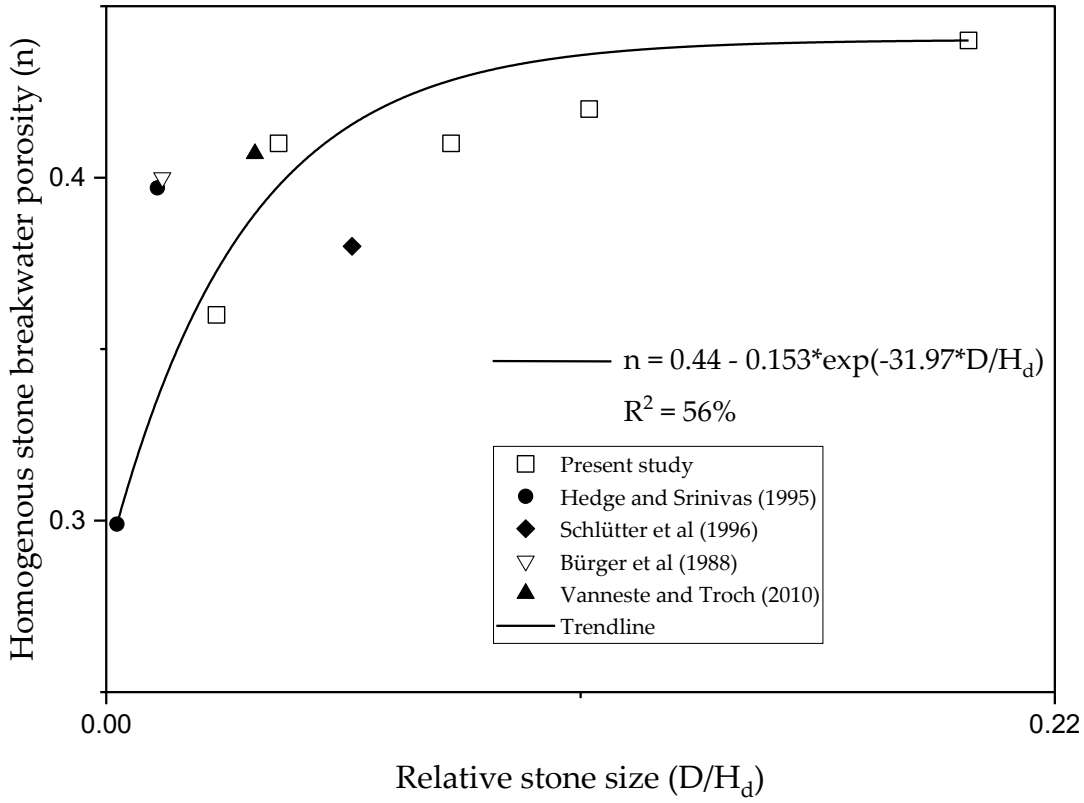

Figure 6.1 Relationship of relative stone size and structural porosity

In this study, the measured porosity data are presented in relation to the relative stone size (D/H_d) and porosity (n) in **Table 6.1**. This information provides a comprehensive understanding of how porosity varies with different stone sizes in coastal structures. Additionally, the study compares the measured porosity values obtained in this research with porosity data from other researchers, as shown in **Figure 6.1**. This comparison allows for further insights and validation of the porosity measurements.

By understanding and quantifying the porosity of coastal structures, researchers and engineers can make informed decisions regarding the design, construction, and maintenance of these structures. Proper porosity management can help optimize sediment transport processes, minimize scour potential, and ensure the long-term stability and functionality of coastal infrastructure.

6.2 Wave dissipation due to porous structures

In this chapter, special attention was given to controlling the initial conditions to ensure consistency and repeatability of the experimental runs. The initial profile of the bed in the scour area and the initial water level were closely monitored and controlled. Three repetitions were conducted for each case, involving a specific sediment size and stone size, to validate the repeatability of the results.

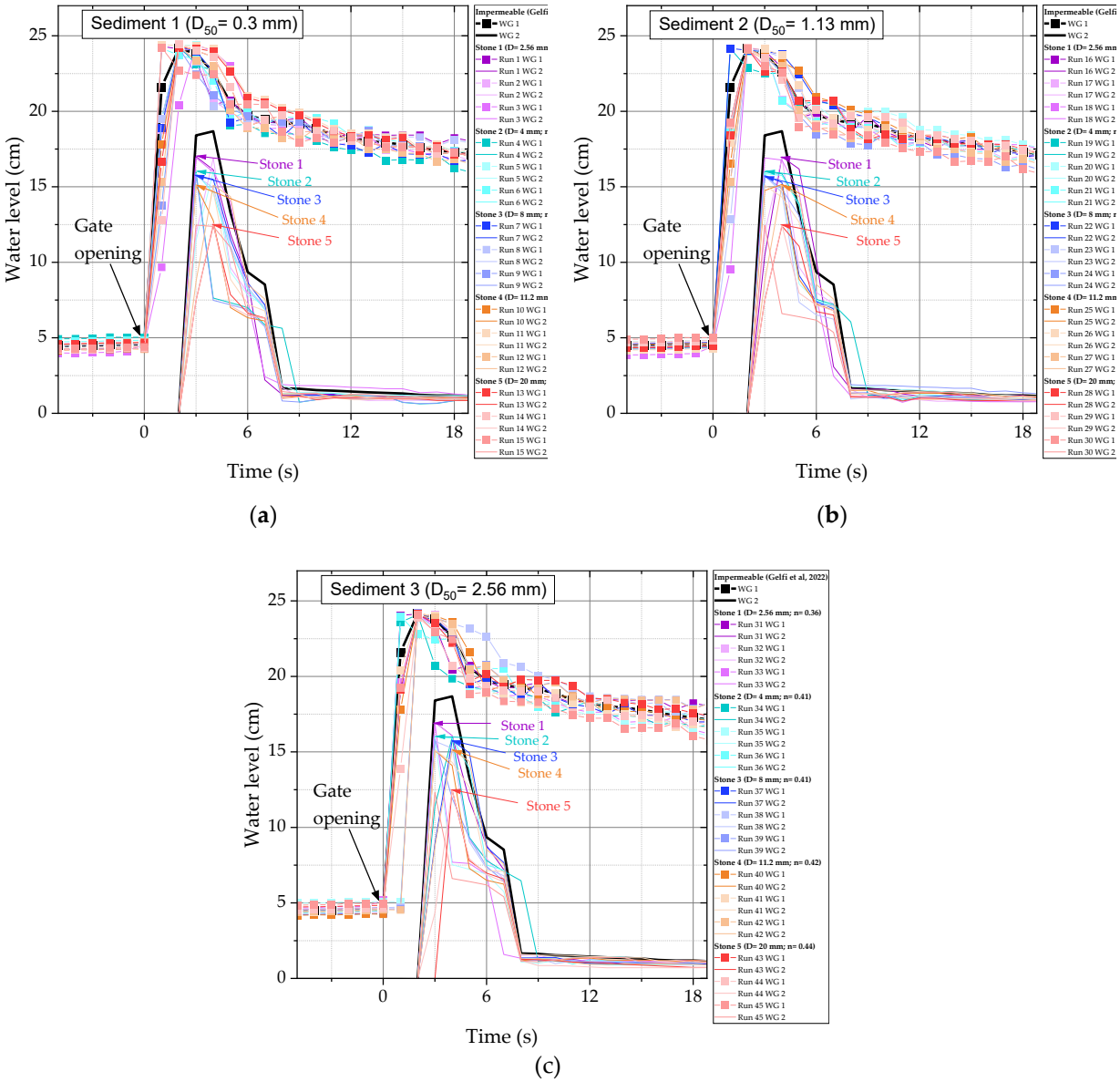

Figure 6.2 Water level variation in the flume: a) sediment 1; b) sediment 2; c) sediment 3

Figure 6.2 illustrates the variation in water level in the flume for WG1 and WG2. Additionally, the water level variation for the impermeable case, obtained from the study by Gelfi et al. (2022), is also provided for comparison. The results show that the presence of a porous structure, compared to an impermeable one, reduces the inundated wave height at WG2 by up to 27%. However, for WG1, where the conditions were the same for both impermeable and porous structures, similar water profiles were observed.

The average inundated wave heights at WG2 for different stone sizes are as follows: stone 1 (D= 2.56 mm; n= 0.36) with an average height of 16.94 cm, stone 2 (D= 4 mm; n= 0.41) with 15.94 cm, stone 3 (D= 8 mm; n= 0.41) with 15.74 cm, stone 4 (D= 11.2 mm; n=

0.42) with 15.06 cm, and stone 5 (D= 20 mm; n= 0.44) with 12.44 cm. Generally, it can be observed that larger stone sizes (corresponding to higher structural porosity) tend to decrease the inundation wave height.

The difference in average inundated wave height between stone 1 (n= 0.36) and stone 5 (n= 0.44) is approximately 4.5 cm (which translates to around 2.25 m in real scale). This difference is quite significant, especially considering the experimental scale of 1:50. It is important to note that wave inundation height (H_d) is a crucial variable in predicting landward scour depth (D_s) according to Equation 1. Therefore, the analysis of landward scour cannot disregard the examination of structural porosity, as it plays a significant role in influencing wave inundation and subsequent scour processes.

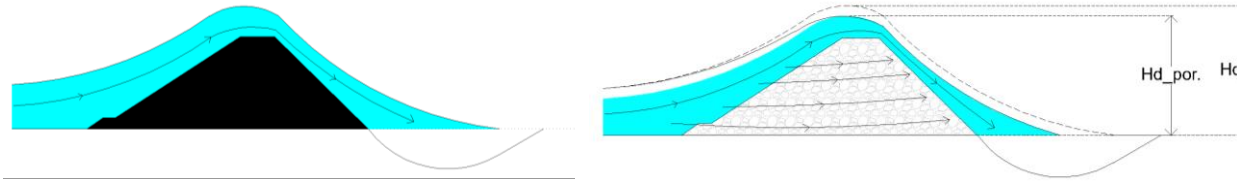

(**a**) (**b**)

Figure 6.3 Inundated wave mechanism over: a) impermeable structure; b) porous structure

The wave is fully transmitted when the reaching impermeable structure. This situation generated higher inundated wave height (h) reaching the landward scour medium (**Figure 6.3a**). However, if permeable coastal structure model is considered, waves will be dissipated to some extent reducing the transmitted wave height (Ting et al, 2004). **Figure 6.3b** illustrates the mechanism of dissipated flow through porous structure that create lower inundated wave height in the scour medium based on experimental results.

6.3 Scour profiles and relative scour depth

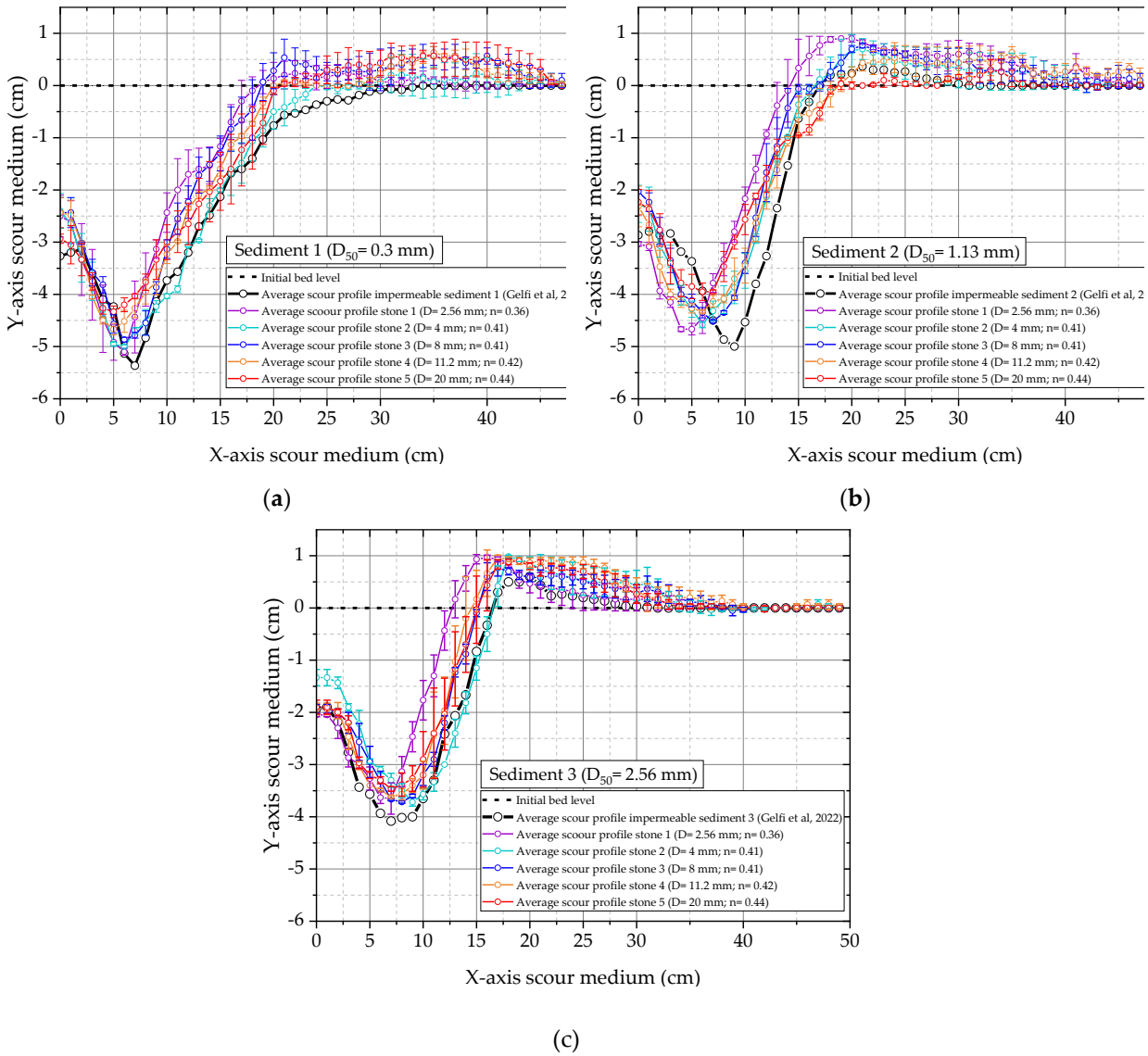

Figure 6.4 Landward scour profiles for a) sediment 1; b) sediment 2; c) sediment 3

Figure 6.4 displays the average developed landward scour profiles for each case, along with error bars. The corresponding impermeable case is also included in black, based on the study by Gelfi et al. (2022). Overall, it can be observed that the presence of porous structures tends to shift the scour profile closer to the direction of the structure (seaward).

In terms of scour depth (D_s), it is evident that the reduction in scour depth is proportional to the increase in structural porosity (n). This implies that higher porosity in the coastal structures leads to a shallower scour depth. The error bars provide an indication of the variability in the scour depth measurements across the repetitions for each case.

The comparison with the impermeable case provides a reference point for evaluating the effectiveness of porous structures in mitigating landward scour. The results demonstrate that the introduction of porosity in the coastal structures has a noticeable influence on the

landward scour profile, resulting in reduced scour depths. This finding further emphasizes the importance of considering structural porosity when analyzing and designing coastal structures to minimize scour-related issues.

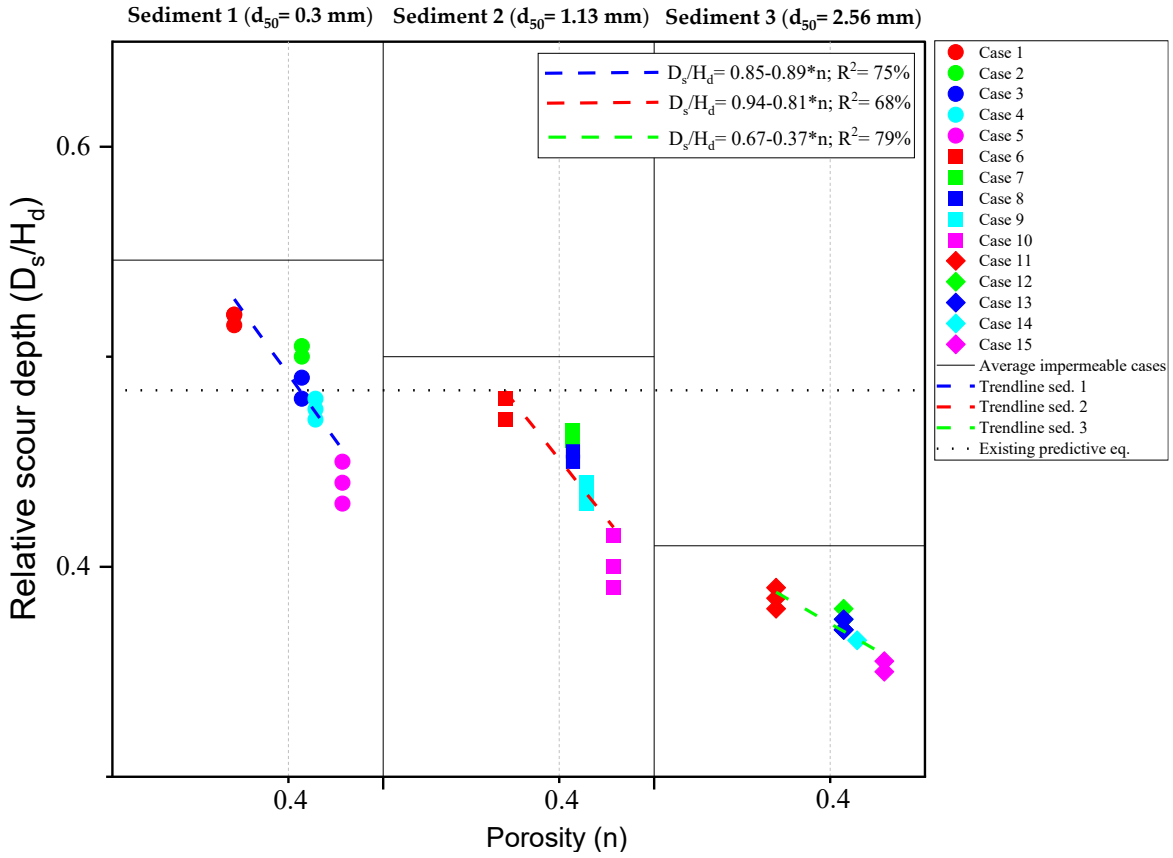

Figure 6.5 Relationship of structural porosity and relative scour depths

Figure 6.5 illustrates the relationship between structural porosity (n) and relative landward scour depth (D_s/H_d) as measured in the laboratory. Generally, a linear reduction trend in scour depth (D_s) can be observed with increasing structural porosity within the range of n=0.36-0.44. The data points for impermeable structures are also included, based on previous research experiments. However, it should be noted that data beyond a porosity of 0.44 and below 0.36 are not applicable due to practical limitations. The existing predictive equation proposed by Jayaratne (2016) is represented by the dash dot-black line, which provides a single value for all cases without considering structural porosity.

6.4 Towards further improvement of the predictive equation

For all sediments tested, we can observe the linear trend patterns of relative scour depth (D_s/H_d) follow the following formula,

$$\frac{D_s}{H_d}(n) = A - B * n \tag{6-1}$$

where A is a intercept constant and B is a gradient function constant. Since there are 3 sediment sizes treated, Figure 6.6 shows the relation relative sediment size (d_{50}/H_d) to the earlier constants. Therefore, the constants A and B is:

$$A = 0.77 - 2.97x10^{-4}x\frac{H_d}{d_{50}} \tag{6-2}$$

$$B = 0.49 - 0.0013x\frac{H_d}{d_{50}} \tag{6-3}$$

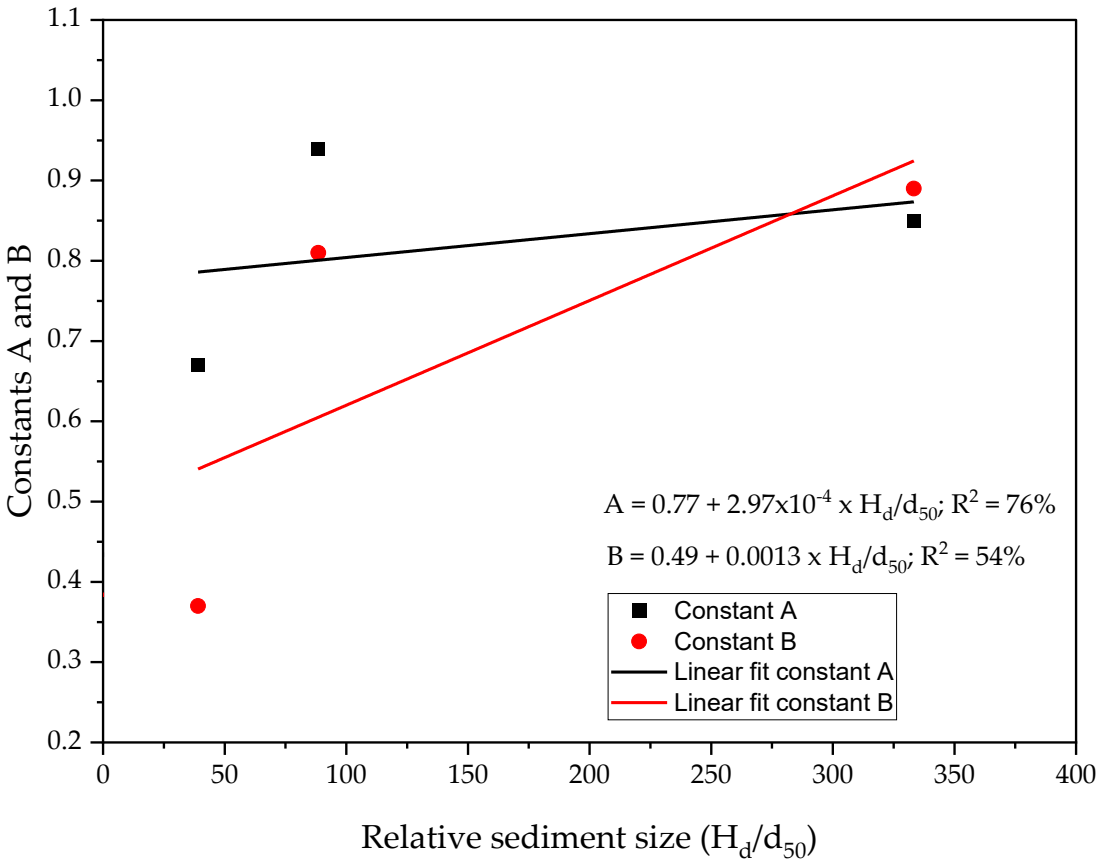

Figure 6.6 Relationship of relative sediment size (d_{50}/H_d) and constants

Hence,

$$\frac{D_s}{H_d}(n, d_{50}) = \left[0.77 - 2.97x10^{-4}x\frac{H_d}{d_{50}}\right] - \left[0.49 - 0.0013x\frac{H_d}{d_{50}}\right] * n \tag{6-4}$$

Treating the current trends as a deviation to the predicted value and normalize them will produce the improved predictive equation ($\lambda_{n,s}$) as a function of sediment size (d_{50}) and porosity (n),

$$\lambda_{n,s} = \frac{\frac{D_s}{H_d}(n, d_{50})}{\left(\frac{D_s}{H_d}\right)_0} \tag{6-5}$$

$$\lambda_{n,s} = 1.24 - 1.61n\left(0.49 - 0.0013\frac{H_d}{d_{50}}\right) - 0.00048\frac{H_d}{d_{50}} \tag{6-6}$$

The relation of porosity (n) and relative stone diameter (D/H_d) can be extracted from **Figure 6.1** as follows,

$$n = 0.44 - 0.153 * \exp\left(\frac{-31.97D}{H_d}\right) \tag{6-7}$$

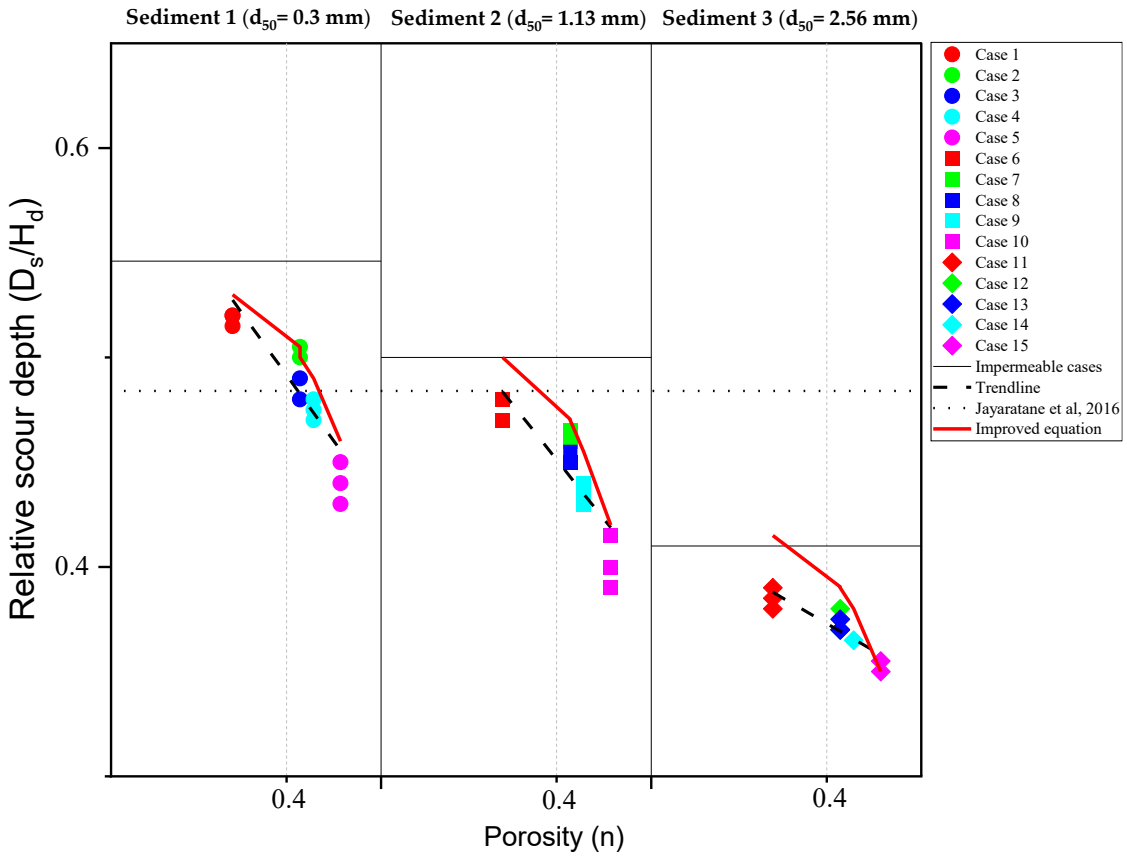

Figure 6.7 Applying improved fitted coefficient considering d_{50} and n effect

Figure 6.7 shows the application of improved fitted coefficient of existing predictive equation considering area of validity:

1. Sediment size (d_{50})= 0.3-2.56 mm
2. Structural porosity (n)= 0.36-0.44

In general, we can see a good agreement (R^2= 75%) (red lines) to the experiment dataset.

6.5 Conclusion

In this chapter, we conducted experiments to examine the impact of coastal structural porosity (n) on local scours behind coastal structures. Porosity, which refers to the amount of void space within a material, plays a crucial role in influencing the flow of water and sediment around coastal structures. By manipulating the porosity of model structures and measuring the resulting scour depth, our objective was to gain a better understanding of how this property affects scour processes. The analysis presented in this chapter represents one approach for utilizing the experimental results, involving the incorporation of the structural porosity effect into the fitted coefficient (λ). However, the interaction between porosity (n)

and the other parameters has been understated and overlooked. This aspect requires thorough consideration in future research endeavors.

The findings of our experiments provide valuable insights that can contribute to the design and construction of real-world coastal structures, which are often susceptible to scour and erosion. Understanding the relationship between porosity and scour depth can help engineers and designers make informed decisions regarding the selection of materials and the incorporation of porosity-enhancing features to mitigate scouring effects. These findings have practical implications for improving the stability and longevity of coastal structures and contribute to the broader field of coastal engineering.

Chapter 7
Concluding Remarks

7. Concluding Remarks

7.1 Summary of the study

The laboratory experiments conducted in this study have highlighted the influence of sediment size (d_{50}) and structural porosity (n) on local scour behind the structure. The existing predictive depth equation did not explicitly account for this effect and provided a single value for scour depth regardless of the sediment and structural porosity variability.

Through our investigation, we observed a correlation between the median sediment size (d_{50}), structural porosity (n) and the observed scour depth (D_s), which followed an exponential relationship. By normalizing the fitted coefficient (λ) in the existing equation to obtain the updated fitted coefficient ($\lambda_{n,s}$) as a function of d_{50} and n, we have incorporated those variables into the updated predictive equation, thereby improving its performance in predicting scour depths.

The simulation of the phenomenon by using XBeach was successful in capturing the changes in water level resulting from the dam-break mechanism. However, it tended to overestimate the morphodynamical aspects, possibly due to an overestimation of the simulated flow velocity. To mitigate this issue, the study introduced the soil dilatancy effect by increasing the critical shield parameter through higher porosity in the sheared zone (n_l) or using the pormax function. This adjustment led to an improvement in the agreement between the simulated erosion volume and the experimental results.

Nevertheless, the study also identified limitations in accurately predicting the scour depth (D_s) using the XBeach model. Further refinements and improvements are necessary to achieve better alignment between the simulated scour depths and the experimental data. Overall, this study provides valuable insights into the capabilities and limitations of the XBeach model for simulating landward scour. It highlights the potential of utilizing the soil dilatancy effect to enhance the model's performance but also underscores the need for ongoing research and development in this field.

7.2 Future recommendations

Indeed, this study acknowledges that it focuses on 2 specific aspects of the existing practical predictive depth equation proposed by Jayaratne et al (2016), namely sediment size (d_{50}) and structural porosity (n). The uncertainties associated with the equation extend

beyond those factors, including filling mechanism of incoming waves, structural mechanism, etc.

Considering additional variables would contribute to a more comprehensive understanding of the scour process. Furthermore, conducting experiments at a larger geometrical scale is recommended to minimize the scale effects that may exist in the laboratory experiments conducted in this study. Scaling up the experiments can provide a more accurate representation of real-world conditions and help improve the predictive capabilities of the equation.

As for numerical investigation, XBeach still cannot predict the scour depth accurately even though soil dilatancy effect has set maximum. It is recommended to investigate bed friction factor between the flow and structure so that simulated flow velocity in the scour medium can be reduced and presumably underestimate the scour depth as well. A higher model resolution (3D simulation) is also highly recommended to incorporate more factors (such as turbulence) and enhance the reliability of the model.

Furthermore, we encourage to validate the dataset of the effect of structural porosity to landward scour numerically in the future. To do so, Lagrangian type model will be more suitable as opposed to XBeach which is Eulerian model.

References

Sediment size effects:

1) Bormann, N. E. and Julien, P. Y. : **Scour downstream of grade-control structures**, *J. of Hyd. Eng.*, Vol. 117, No. 5, pp. 579–594, 1991.
2) Bricker, J. D. et al : **Scour depths near coastal structures due to the 2011 Tohoku Tsunami**, *J. of Hydr. Research*, Vol. 50. No. 6, pp. 637–641, 2012.
3) Chanson, H. : **Tsunami surges on dry coastal plains: Application of dam break wave equations**, *Coast. Eng. J.*, Vol. 48, No. 4, pp. 355–370, 2006.
4) Chen, J. et al. : **Laboratory study on protection of tsunami-induced scour by offshore breakwater**, *Nat. Hazards,* Vol. 81, No. 2, pp. 1229-1247, 2015.
5) Crowley, R. et al : **An examination of the dependency between max. equilibrium local scour depth and the grain size/structure size ratio**, *Water*, Vol. 12, No. 11, pp. 1-12, 2020.
6) Goseberg, N. et al : **Laboratory-scale generation of tsunami and long waves**, *Coast. Eng.*, Vol. 79, pp. 57–74, 2013.
7) Guan, D. et al. : **Local scour at offshore windfarm monopile foundations** : A review, *Water Science and Engineering*, Vol. 15, No. 1, pp. 29–39, 2022.
8) Hughes, S.A. : **Physical models and laboratory techniques in coastal engineering**, *World Scientific*, Scientific Publishing Co. Pte. Ltd., Singapore (November), 1993.
9) Jayaratne, M. P. R. et al. : **Failure mechanism and local scour at coastal structures induced by tsunami**, *Coast. Eng. J.*, Vol. 58, No. 4, pp. 1-38, 2016.
10) Krautwald, C. et al. : **Eng. lessons from sept. 28, 2018 Indonesian tsunami: scouring mechanisms and effects on Infr.**. *J. of Waterway, Port, Coast., and Ocean Eng.*, Vol. 147, No. 2, pp. 1-16, 2021.
11) Karim, O. A. and Ali, K. H. M. : **Prediction of flow patterns in local scour holes caused by turbulent water jets**. *Journal of Hydraulic Research*, Vol. 38, No. 4, pp. 279–287, 2000.
12) Lee, S. O. and Sturm, T. W. : **Effect of sediment size scaling on physical modeling of bridge pier scour**, *J. of Hydr. Eng.*, Vol. 135, No. 10, pp. 793–802, 2009.
13) Sumer, B. M. and Fredsoe., J. : **Experimental study of 2D scour and its protection at a rubble-mound breakwater**, *Coastal Eng.*, Vol. 40, pp. 59-87, 2000.

14) Mitobe, Y. et al. : **Experiments on local scour behind coastal dikes induced by tsunami overflow**, *Coast. Eng. Proc.,* 2014.

Numerical simulations (XBeach):

15) MLIT of Japan. : **White paper on land, infrastructure, transport and tourism in** Japan, 2011.
16) Robertson, I. N. et al : **Exp. results of tsunami bore forces on structures**, *Proc. of the Int. Conf. on OMAE*, pp. 509–517, 2008.
17) de Vet, P. L. M., : **Modelling dune erosion, overwash & breaching at fire island (NY) during hurricane sandy**. *The Proceeding of Coastal Sediments 2015*, World Scientific, 2015.
18) Elsayed, S. M., & Oumeraci, H : **Effect of beach slope and grain-stabilization on coast. sediment transport: An attempt to overcome the erosion overestimation by XBeach**, *Coast. Eng.*, Vol. 121, pp. 179–196, 2017.
19) Gelfi et al. : **Sediment size effect on the landward coastal structure scour prediction due to tsunami**, *J. of Japan Society of Civil Engineers, Ser. B2 (Coast. Eng.),* Vol.. 78, No. 2, pp. 469-474, 2022.
20) McCall, R. T. et al. : **2D time dependent hurricane overwash and erosion modeling at Santa Rosa Isl.**, *Coast. Eng.*, Vol. 57, pp. 668–683, 2010.
21) Roelvink, D. et al : **Modeling storm impacts on beaches, dunes & barrier island**, *Coast. Eng.*, Vol. 56, pp. 1133–1152, 2009.
22) van Rijn, L. C. : **Unified view of sediment transport by currents and waves. II: Suspended transport**, *J of Hydr. Eng.*, Vol. 133, No. 6, pp. 668–689, 2007
23) van Rijn, L. C. : **Unified view of sediment transport by currents and waves. III : Graded beds**, *J. of Hydr. Eng.*, Vol. 133, No. 7, 761–775, 2007.
24) van Rijn, L. C. : **Unified view of sediment transport by currents and waves. I: Initiation of motion, bed roughness, and bed-load transport**. *J. of Hydr. Eng.*, Vol. 133, No. 6, pp. 649–667, 2007.
25) van Rijn, L. C. : **Sediment transport. Part I: Bed load transport**. J. of Hydr. Eng., Vol. 110, No. 10, pp. 1431–1456, 1984.
26) van Rhee, C. : **Sediment entrainment at high flow velocity**. *J.l of Hydr. Eng.*, Vol. 136, No. 9, pp. 572–582, 2010.
27) van Rijn, L. C. : **The predictability of cross-shore bed evolution of sandy beaches at the time scale of storms and seasons using process-based profile models**, *Coast. Eng.*, Vol. 47, No. 3, pp. 295–327, 2003.
28) **XBeach Documentation Release v1.23.5527, 2018**.

Structural porosity effects:

29) Ali, A., & Tanaka, N. (2020). **Experimental study of scouring downstream of coastal vegetation in an inundating tsunami current**. Landscape and Ecological Engineering, 16(4), 273–287.
30) Breusers, H. N. C., Nicollet, G., & Shen, H. W. (1977). **Erosion locale autour des piles cylindriques**. Journal of Hydraulic Research, 15(3), 211–252.
31) Ismail, H., Xu, Y., & Liu, X. (2021). **Flow and Scour around Idealized Porous Engineered Log Jam Structures**. Journal of Hydraulic Engineering, 147(1), 04020089.
32) Kim, H. S., Kimura, I., & Shimizu, Y. (2016). **Experimental investigations of scour pools around porous obstructions**. Water (Switzerland), 8(11).
33) Madsen, O. S., & White, S. M. (1976). **Transmission Characteristics of Porous Rubble -Mound Breakwaters**. Miscellaneous Report No. 76-5, 146p.
34) MELLINK, B. (2012). **Numerical and experimental research of wave interaction with a porous breakwater**. 1230166.
35) Nishimura, H. (1978). **Scouring at the toe of a seawall due to tsunamis**. Coastal Engineering 1978, 2540–2547.
36) Rahman, M. A., & Akter, A. (2014). **The Effect of Porosity of Submerged and Emerged Breakwater on Wave Transmission**. International Journal of Environmental Science and Development, 5(5), 473–478.
37) Reis, M. T., Neves, M. G., & Hu, K. (2009). **Wave overtopping of a porous structure: Numerical and physical modeling**. Journal of Coastal Research, SPEC. ISSUE 56, 539–543.
38) Ting, C. L., Lin, M. C., & Cheng, C. Y. (2004). **Porosity effects on non-breaking surface waves over permeable submerged breakwaters**. Coastal Engineering, 50(4), 213–224.
39) Torres-Freyermuth, A., Brocchini, M., Corvaro, S., & Pintado-Patiño, J. C. (2017). **Wave attenuation over porous seabeds: A numerical study**. Ocean Modelling, 117(October), 28–40.
40) Vanneste, D. F. A., & Troch, P. (2011). **Experimental Research on Pore Pressure Attenuation in Rubble-Mound Breakwaters**. Coastal Engineering Proceedings, 1(32), 30.
41) Wan, K., & Xu, Q. (2014). **Local porosity distribution of cement paste characterized by X-ray micro-tomography**. Science China Technological Sciences, 57(5), 953–961.
42) Wu, Y. T., & Hsiao, S. C. (2013). **Propagation of solitary waves over a submerged permeable breakwater**. Coastal Engineering, 81, 1–18.
43) Yu, X., & Chwang, A. T. (1994). **Wave Motion through Porous Structures. Journal of Engineering Mechanics**, 120(5), 989–1008.

List of publications

1. Gelfi et al.: **Sediment size effect on the landward coastal structure scour prediction due to tsunami**, Journal of Japan Society of Civil Engineers, Ser. B2 (Coastal Eng.), Vol. 78, No. 2, pp. 469-474, 2022.
2. Gelfi and Suzuki: **Investigation of Tsunami Induced Landward Scour with XBeach**. Journal of Japan Society of Civil Engineers, Ser. B3 (Ocean Eng.), Vol. 79, No. 18.
3. (Expected to be Submitted in July 2023) Gelfi et al: **Structural Porosity Effects to the Landward Coastal Structure Scour due to Tsunami**. Coastal Engineering Journal.